Supporting Information

Analysis of the Charge Generation and Recombination Processes in the PM6:Y6 Organic Solar Cell

Saied Md Pratik, Grit Kupgan, Jean-Luc Brédas,* and Veaceslav Coropceanu*

Department of Chemistry and Biochemistry
The University of Arizona
Tucson, Arizona, 85721-0041, USA

* Corresponding authors: coropceanu@arizona.edu; jlbredas@arizona.edu

Contents

Section SA: Methodology

1. Computational details

We performed all-atom molecular dynamics (MD) simulations for the PM6:Y6 (*i.e.,* donor:acceptor) blend with the LAMMPS package using the OPLS-AA (optimized potentials for liquid simulations-all atom) force field.[1-4] To accurately describe the intra and inter-molecular interactions, we parameterized the generalized OPLS-AA force field using long-range-corrected DFT calculations for atomic charges, bond lengths, bond angles, and dihedral angles of PM6 and Y6. In the case of PM6, we considered its trimeric unit and used the middle unit for the parameterization. The atomic charges were obtained by fitting the DFT electrostatic potential calculated at the ωB97X-D/cc-PVTZ level of theory.[5, 6] Bond lengths and angles were directly taken from the PM6 and Y6 molecules optimized at the ωB97X-D/6-31G(d,p) level, keeping the harmonic force constants unchanged. Dihedral parameters between the core and end-groups were

fitted based on DFT-scanned torsion potentials at the ωB97X-D/6-31G(d,p) level of theory.[7] These DFT calculations were carried out using the Gaussian 16 package.[8]

The PM6:Y6 blends used for analysis were obtained by following multiple stages of isothermal-isobaric ensemble MD (NPT-MD). Firstly, we randomly placed 10 polymeric chains of PM6 consisting of 20 repeat units and 200 molecules of Y6 in an empty cubic simulation box of length 500 Å within periodic boundary conditions (density of ~0.1 g/cm^3) using the Polymatic code.[9] Then, 30 ns of NPT-MD was performed at 650 K and 1 atm to equilibrate the system. Subsequently, the blend was cooled from 650 K to 300 K at 1 atm at a rate of 10 K/ns. Then, the system was allowed to equilibrate for another 30 ns of NPT-MD at 300 K and 1 atm to obtain the amorphous films. We finally considered the last 10 ns of the NPT-MD for further analysis. The Velocity Verlet algorithm with 2 fs timestep was used in all MD simulations and the pressure and temperature were controlled using Nose-Hoover barostat and thermostat. The van der Waals interactions were taken into account using a cutoff of 12 Å, with the particle–particle–particle–mesh (pppm) used for the electrostatics term. We conducted a total of three independent simulations of the PM6:Y6 blend, so as to prevent any bias in terms of initial configurations.

To perform the electronic-structure calculations, we extracted 3000 PM6:Y6 molecular complexes (1000 from each box) consisting of dimeric-PM6 chains and Y6 molecules from snapshots of the MD simulations using the Pysimm tool.[10] These complexes are extracted based on a 'close contact' criterion (see Figure S1a), where each close contact corresponds to an interatomic distance of less than 4 Å between PM6 and Y6 atoms (see reference [11] for further details). In addition, we collected 1500 PM6:2Y6 complexes (500 from each box), comprising dimeric-PM6 and two Y6 molecules, from MD snapshots using the same 'close contact' criterion. We note that the selection of complexes within both PM6:Y6 and PM6:2Y6 were conducted in an

unbiased manner, as evidenced by the wide distribution of center-of-mass to center-of-mass distances ($d_{c\text{-}c}$) between the PM6 and Y6 molecules and between PM6 and 2Y6 (see Figure S2). To capture dynamic disorder, we extracted 200 configurations from each of ten randomly selected PM6:Y6 complexes (thus, totaling 2000 configurations), at intervals of 30 fs, from the trajectories of the MD simulations. The excited-state properties were evaluated at the TDA-DFT level of theory described below and subsequently σ_D was accessed. The σ_S value was then derived from $\sigma_S = \sqrt{\sigma_T^2 - \sigma_D^2}$ (where σ_T is the total disorder). Detailed computational methods for this analysis are given elsewhere.[12-14]

Furthermore, to analyze the distribution of Y6 energetics, we gathered 1000 monomers and 1000 dimers of Y6 by isolating Y6 and 2Y6 from PM6:Y6 and PM6:2Y6 complexes, respectively.

The excited-state calculations were performed using time-dependent DFT (TDDFT) based on the Tamm-Dancoff approximation (TDA). We used the long-range corrected ωB97X-D functional and 6-31G(d,p) basis set, where range-separation parameter (ω) was set to 0.01 $Bohr^{-1}$ based on our previous work.[15-17] In the course of the TDA-DFT calculations, we considered an implicit dielectric environment based on the polarizable continuum model (PCM) with a dielectric constant (ε) value of 3.0, which is commonly used for organic solar cells. The electronic couplings between the ground states (and local-exciton states) and the CT states were obtained using the fragment charge difference method, which is based on the generalized Mulliken-Hush approach.[18, 19] We note that the long-side alkyl chains in both PM6-oligomer donor and Y6 acceptors were substituted with -CH_3 groups for these calculations to reduce computation costs. All the excited-state calculations were carried out using the Q-Chem 5.4.0 package.[20]

We note that in PM6:2Y6 complexes the number of triplet states below the first ^{3}CT state is doubled compared to PM6:Y6, resulting in four low-lying triplet states instead of two; this is

simply due to the presence of two Y6 molecules. Many PM6:2Y6 complexes show degenerate T_1 and T_2 states, with some showing minor splitting due to the structural differences between the two Y6 molecules; the same is true for T_3 and T_4 states. Since, the T_1 and T_2 states in PM6:2Y6 are analogous to the T_1 state in PM6:Y6 and the T_3 and T_4 states in PM6:2Y6 correspond to the T_2 state in PM6:Y6, we combined T_1 with T_2 and T_3 with T_4 to keep our discussion simple and to better analyze their local/CT character.

The radiative rate (k_r) from the ^{1}LE(^{1}EX) state to GS in PM6:Y6 (PM6:2Y6) was computed from the Einstein coefficient relation (equation 1)[21]:

$$k_r = \frac{f \times E^2 \times f(n)}{1.499} \quad \text{(S1)}$$

where *f* represents the oscillator strength and E corresponds to the energy of the ^{1}LE (or ^{1}EX for PM6:2Y6) state in cm^{-1}. The factor *f(n)*, defined as $f(n) = \frac{n(n^2+2)^2}{9}$, takes into account the local-field effect on emission intensity and relies on the refractive index (n) of the blend. Here, we considered a typical value of 1.4 for the refractive index, which is commonly observed in the active layers of organic solar cells.

The non-radiative electron transfer rates are calculated using the following equation[22]:

$$k = \frac{2\pi}{\hbar} t^2 \rho(E_f) \quad \text{(S2)}$$

where *t* denotes the electronic coupling, $\hbar$ is the reduced Plank constant, and $\rho(E_f)$ is the density of final states and summing over all probability densities. Within the semiclassical Marcus – Levich – Jortner (MLJ) framework[23], equation 2 can be rewritten as follows:

$$k = \frac{2\pi}{\hbar} t^2 (FCWD) \quad \text{(S3)}$$

Here, FCWD denotes the Franck−Condon-weighted density of states, which is given by:

$$FCWD = \frac{1}{\sqrt{4\pi\lambda_c k_B T}} \sum_{n=0}^{\infty} \frac{e^{-S_{qm}} \times S_{qm}^{\,n}}{n!} e^{\frac{-(\Delta E + \lambda_c + n\hbar\omega_{qm})^2}{4\lambda_c k_B T}} \quad \text{(S4)}$$

where k_B is the Boltzmann constant, T is the temperature set to 300 K, and ΔE is the energy difference between the relevant states; λ_c refers to classical reorganization energy and was taken as:

$$\lambda_c = (\sum \lambda_j)_{initial \to final} \quad \text{(S5)}$$

where the λ_j terms correspond to the reorganization energies for low frequency modes (*i.e.*, <100 cm^{-1}), *initial* and *final* represent the initial and final states, $\hbar\omega_{qm}$ is the vibration energy of the effective high-frequency quantum mode, and S_{qm} is the Huang-Rhys factor that is associated with the reorganization energy from high-frequency modes. ω_{qm} and S_{qm} were taken as follows:

$$\omega_{qm} = \sqrt{\frac{(\sum \lambda_i \omega_i^2)_{initial \to final}}{(\sum \lambda_i)_{initial \to final}}} \quad \text{(S6)}$$

$$\lambda_{qm} = \hbar\omega_{qm} S_{qm} \quad \text{(S7)}$$

where ω_i corresponds to a high-frequency mode, λ_i denotes the reorganization energy associated to an ω_i frequency, and λ_{qm} represents the total reorganization energy from high-frequency modes. The low-frequency vibrational modes with frequencies below 100 cm^{-1} were treated classically, while high-frequency modes (>100 cm^{-1}) were treated quantum mechanically. The calculated reorganization energies and Huang-Rhys factors used for computing the rates are provided in Table S4. The frequency-related calculations were performed with the Gaussian 16 package[8] at the same level of theory as the excited-state calculations.

To evaluate the impact of static disorder (σ_S) on the rates, we accounted for σ_S^2 by adding it to $4\lambda_c k_B T$, where σ_S^2 is determined from the contributions to static disorder from both initial (σ_{S-i}) and final (σ_{S-f}) states, expressed as $\sigma_S^2 = \sigma_{S-i}^2 + \sigma_{S-f}^2$.

In order to estimate the rate constant for an electron hopping from Y6 of a PM6:Y6 complex to an adjacent Y6 molecule (mimicking in this way the charge separation) we used Equation S2, where *t* represents the transfer integral for electron transfer and ΔE the change in electrostatic energy. By taking the average center of mass-to-center of mass distances between the PM6 and two distinct Y6 molecules (one in PM6:Y6 complex and second for the adjacent Y6 molecule) as 13.69 Å and 20.15 Å, respectively, using an dielectric constant of 4, *t* of 21.2 meV (based on previous calculations[11]) and other parameters required for the rate calculation from Table S4, we estimate that the electron hoping rate is about 1.1×10^{11} s^{-1}. We note that this rate varies as function of ε, such as 4.0×10^{10} s^{-1} at ε=3, 1.9×10^{11} s^{-1} at ε =5, and 2.6×10^{11} s^{-1} at ε=6.

2. **Close contact vs center-of-mass to center-of-mass (dc-c); distribution of dc-c distances**

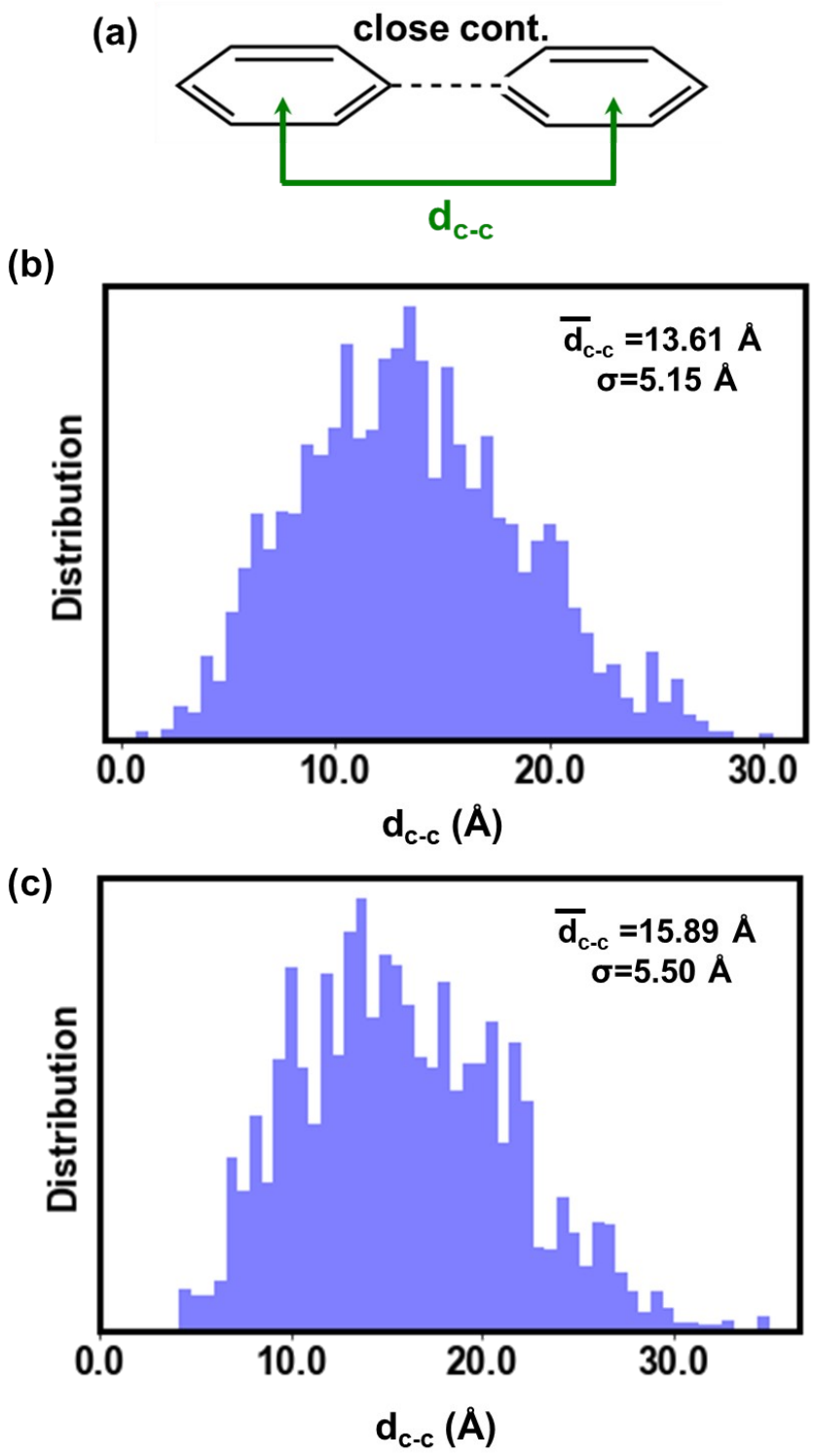

Figure S1: *(a) Schematic representation illustrating the definition of "close contact" and center-of-mass to center-of-mass distances (dc-c). In the example of a benzene dimer, the "close contact" refers to the minimum interaction distance between any two atoms from each benzene ring. In contrast, "dc-c" refers to the distance between the centers of mass of the two benzene rings. Therefore, the "close contact" distance does not correspond to dc-c. (b) Distribution of dc-c values between PM6 and Y6 in PM6:Y6 complexes. (c) Distribution of dc-c values between PM6 and 2Y6 in PM6:2Y6 complexes. The average distance ($\bar{d}_{c-c}$) and standard deviation (σ) are also provided. The broad distribution of dc-c values between PM6 and Y6(2Y6) suggests that the selection of pairs within the PM6:Y6(2Y6) blend was conducted in an unbiased manner, considering various potential interactions between PM6 and Y6(2Y6).*

Section SB: Distributions of state energies and charges in Y6 and PM6:Y6

3. Distributions of singlet and triplet states in Y6

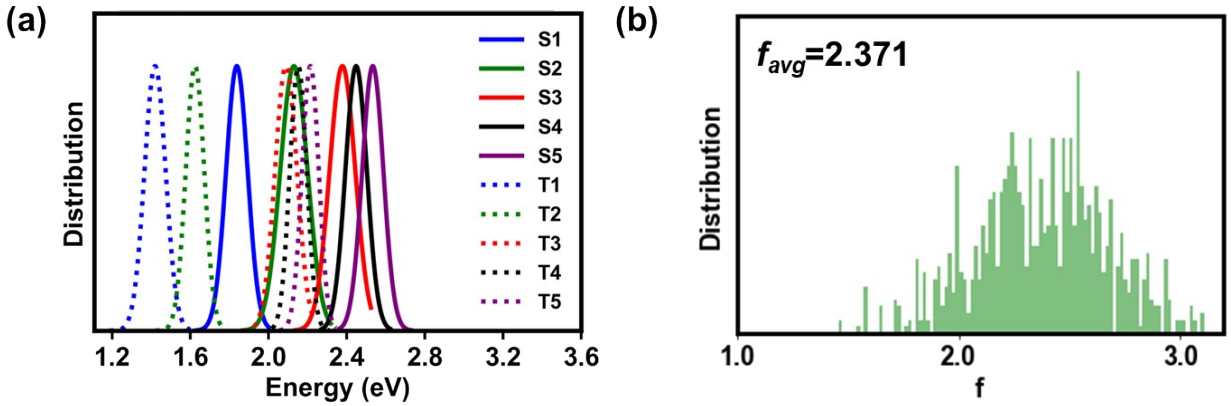

Figure S2: *(a) Normalized energy distribution of singlet and triplet states for Y6. (b) Histogram of the oscillator strengths (f) for the S_1 state, with f_{avg} indicating the average value. These distributions are evaluated based on 1000 Y6 molecules extracted from MD simulations performed on the PM6:Y6 blend, with their excited-state properties calculated at the ωB97X-D/6-31G(d,p) level with ω=0.01 Bohr^{-1} using a PCM model with ε=3.0.*

Table S1: *Average energies E_{avg} (eV) and standard deviations (σ, in eV) of singlet and triplet states in monomeric and dimeric Y6.*

States	Y6 (monomeric)		2Y6 (dimeric)	
	E_{avg}	σ	E_{avg}	σ
S_1	1.84	0.06	1.70	0.09
S_2	2.12	0.07	1.79	0.06
S_3	2.37	0.06	1.85	0.06
S_4	2.45	0.06	1.92	0.07
S_5	2.53	0.06	2.04	0.07
S_6	--	--	2.09	0.06
S_7	--	--	2.15	0.06
S_8	--	--	2.20	0.06
S_9	--	--	2.29	0.06
S_{10}	--	--	2.33	0.06
T_1	1.42	0.06	1.37	0.06
T_2	1.62	0.05	1.44	0.05
T_3	2.08	0.06	1.58	0.05
T_4	2.15	0.05	1.64	0.04
T_5	2.21	0.05	1.76	0.08
T_6	--	--	1.89	0.08
T_7	--	--	2.02	0.06
T_8	--	--	2.06	0.05
T_9	--	--	2.09	0.04
T_{10}	--	--	2.12	0.04

4. Distributions of singlet and triplet states in PM6:Y6 complexes

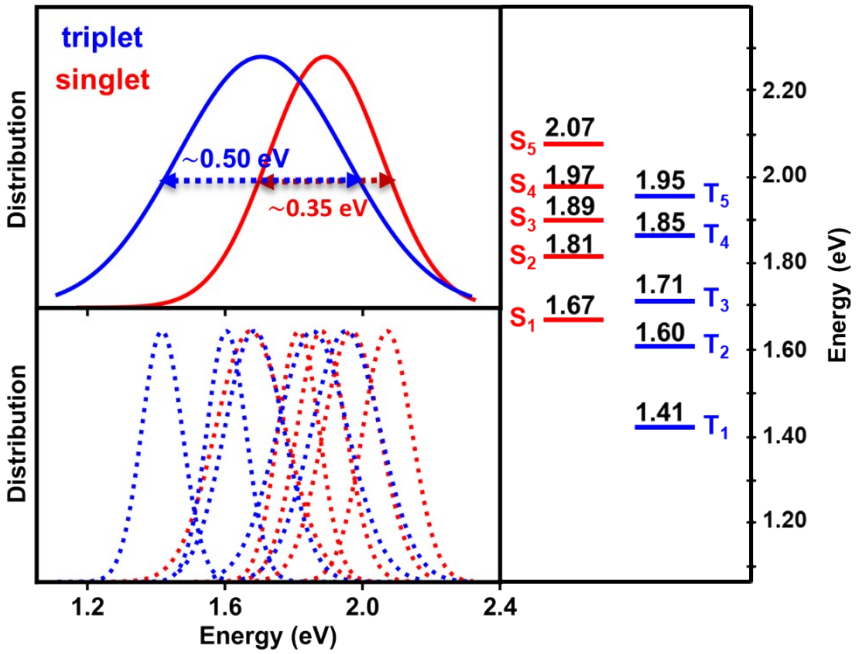

Figure S3: *Normalized energy distributions of the singlet and triplet states in PM6:Y6 complexes based on 3000 MD extracted pairs; the horizontal dotted lines indicate the FWHM of the singlet (red) and triplet (blue) state energies (top left panel), providing the range of the singlet and triplet energy spread; the energy distribution of the constituent states contributing to the overall singlet and triplet distributions is shown in the bottom left panel and their average values are given in the right panel.*

5. Distributions of charges in PM6:Y6

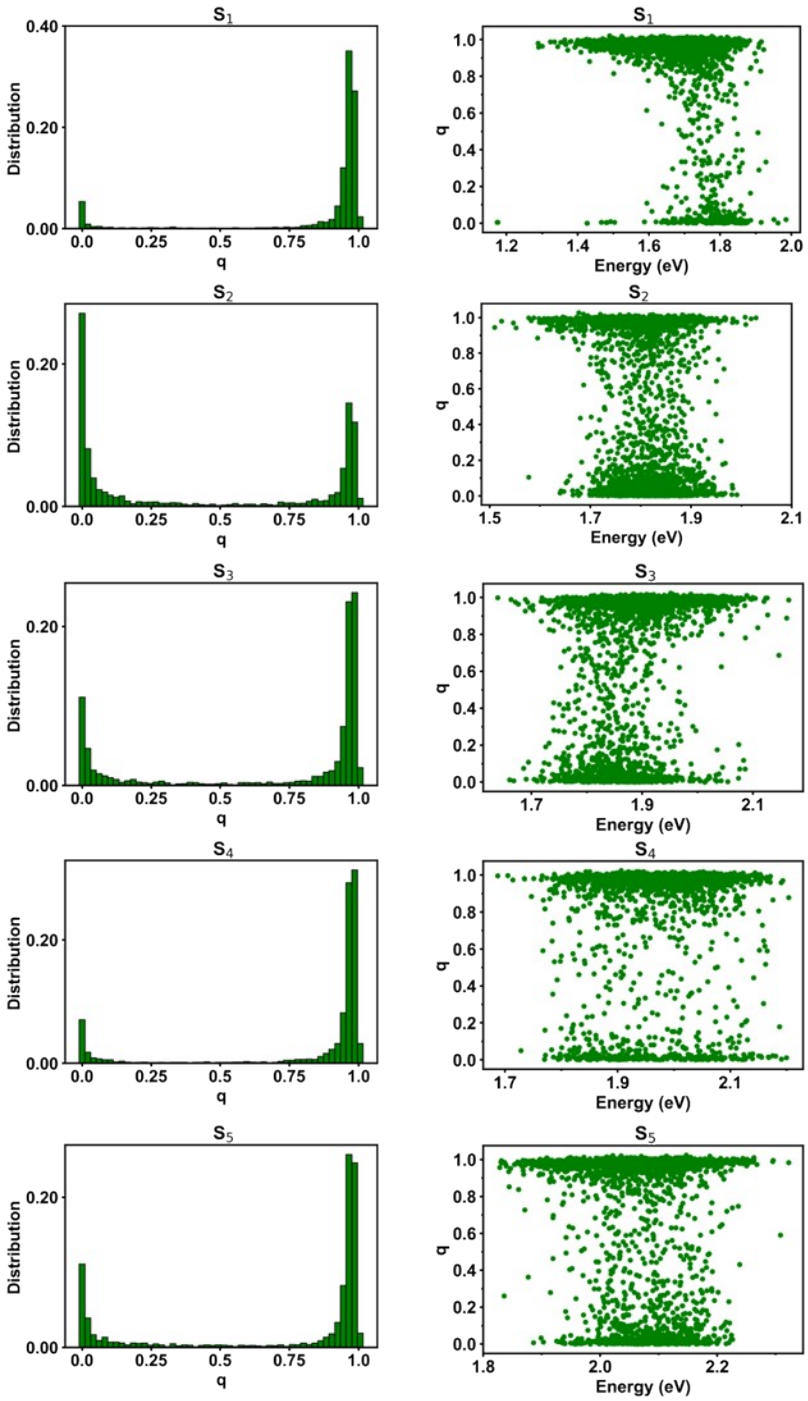

Figure S4: *Histogram plots of charges ("q") and their distribution as a function of energy for various singlet states in PM6:Y6 complexes.*

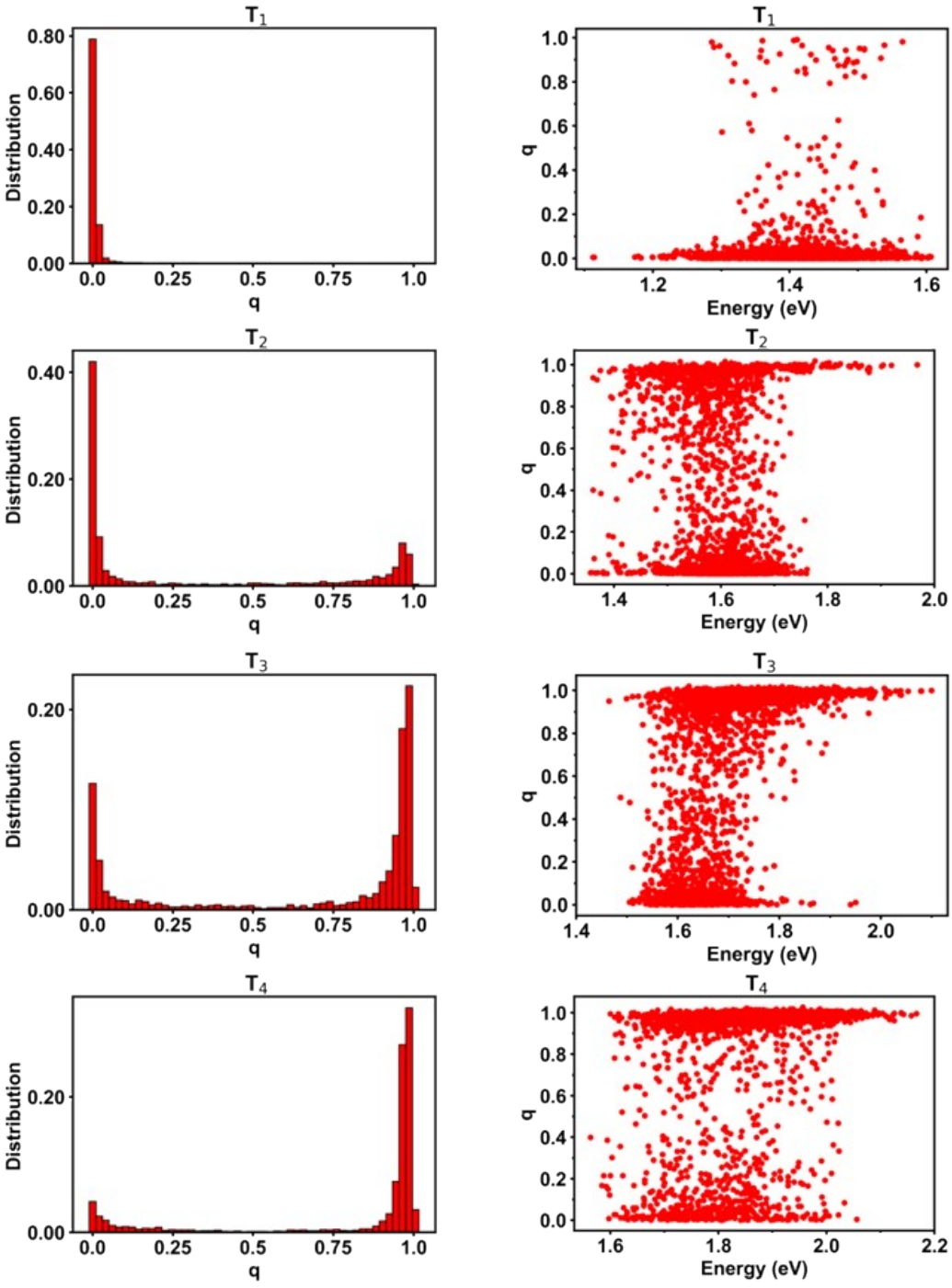

Figure S5: *Histogram plots of charges ("q") and their distribution as a function of energy for various triplet states in PM6:Y6 complexes.*

6. Percentage of LE and CT character in singlet and triplet states

Table S2: *The extent of LE and CT character in singlet and triplet excited states, evaluated for both PM6:Y6 and PM6:2Y6 complexes, based on the q values.*

States	PM6:Y6				PM6:2Y6			
	CT% ($q \geq 0.9$)	LE% ($q \leq 0.1$)	CT% ($q \geq 0.8$)	LE% ($q \leq 0.2$)	CT% ($q \geq 0.9$)	EX% ($q \leq 0.1$)	CT% ($q \geq 0.8$)	EX% ($q \leq 0.2$)
S_1	83.17	7.33	87.53	8.07	62.71	28.15	65.91	29.69
S_2	36.43	43.43	40.10	48.93	43.30	38.49	47.83	41.83
S_3	62.20	20.23	67.13	23.77	33.96	45.30	37.96	49.50
S_4	77.67	10.83	82.07	12.30	30.89	45.30	36.02	49.57
S_5	65.86	18.91	69.36	21.94	34.62	43.36	39.69	47.97
S_6	--	--	--	--	38.21	41.98	42.12	46.23
S_7	--	--	--	--	47.91	34.91	52.29	37.60
S_8	--	--	--	--	57.61	26.08	61.86	29.04
S_9	--	--	--	--	62.94	22.64	66.64	25.20
S_{10}	--	--	--	--	68.40	17.99	72.51	19.68
T_1	0.77	95.70	1.30	97.00	0.73	98.27	1.00	98.73
T_2	22.03	57.03	27.07	60.53	1.93	95.40	2.60	96.33
T_3	57.33	21.70	62.70	25.50	16.88	69.25	19.88	71.98
T_4	76.17	10.27	78.53	13.67	19.41	64.78	22.82	68.45

T_5	80.97	5.17	84.60	7.33	35.82	46.90	40.29	49.17
T_6	--	--	--	--	44.74	38.07	49.53	41.04
T_7	--	--	--	--	51.42	31.87	55.32	35.71
T_8	--	--	--	--	55.39	30.19	59.37	33.09
T_9	--	--	--	--	62.33	23.11	65.70	25.88
T_{10}	--	--	--	--	68.73%	18.67%	71.70	20.49

7. PM6:Y6 complex

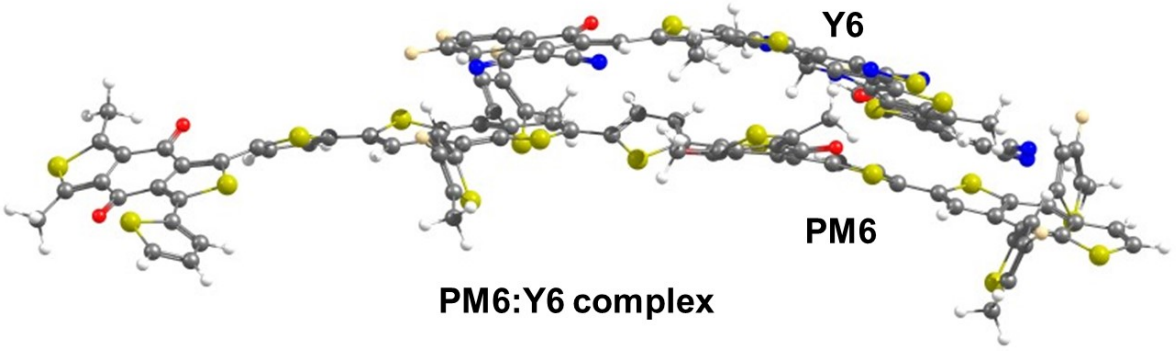

Figure S6: *PM6:Y6 complex taken from MD simulation and further used for NTO calculation.*

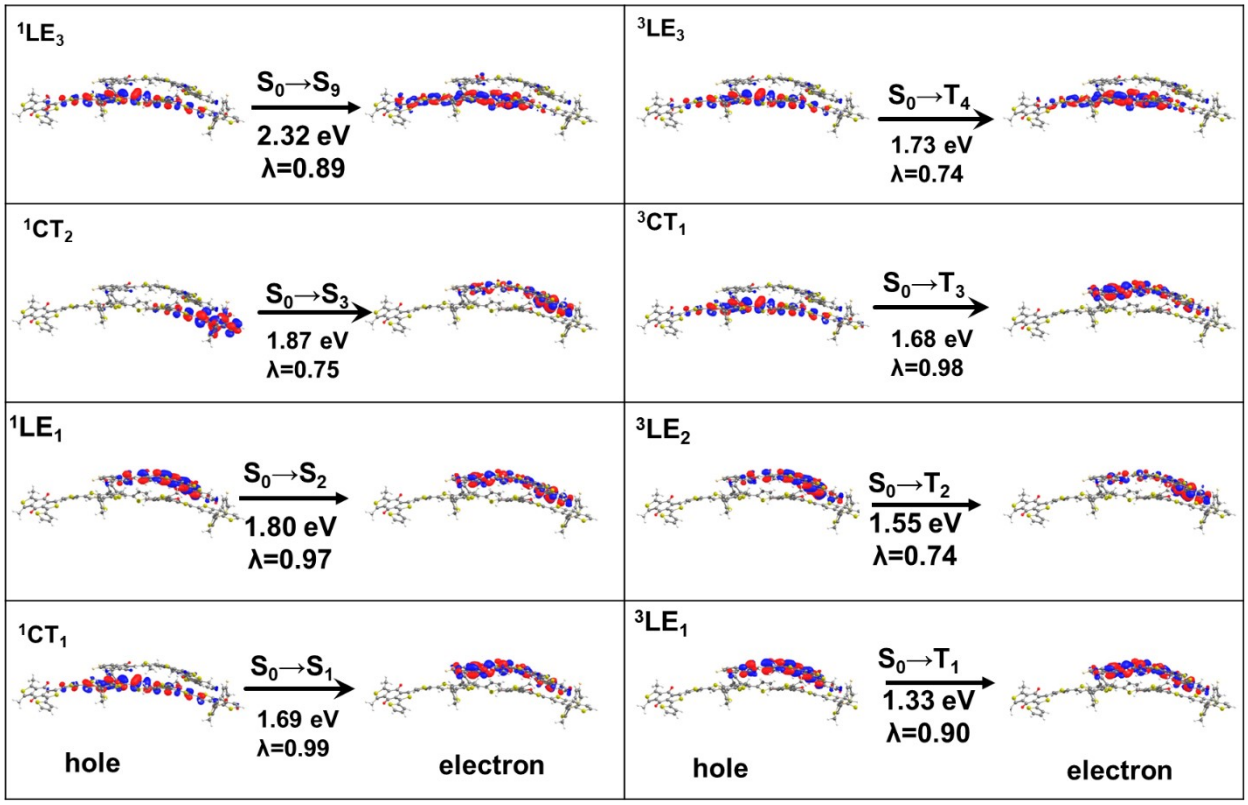

Figure S7: *Hole and electron natural transition orbitals (NTOs) in the representative PM6:Y6 complex (shown in Figure S6) for different singlet and triplet LE and CT states. In the complex, Y6 is at the top and PM6 is at the bottom. Also see section SE for further details.*

8. Energy offsets between singlet CT and triplet CT states

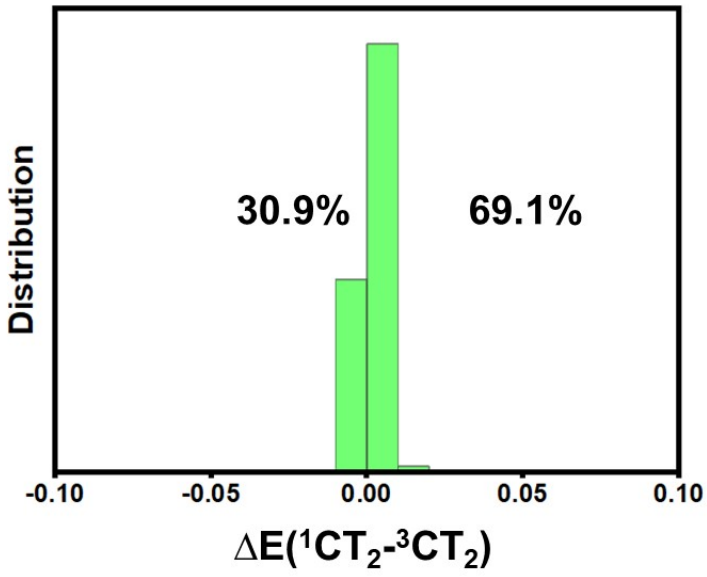

Figure S8: *Distribution of energy offsets (in eV) between singlet and triplet CT_2 states [$\Delta E(^1CT_2$-$^3CT_2)$] across individual complexes for PM6:Y6. The percentages of complexes showing positive and negative energy offsets are also provided.*

Section SC: Disorder and defect states in PM6:Y6

9. Static and dynamic disorders in the PM6:Y6 blend

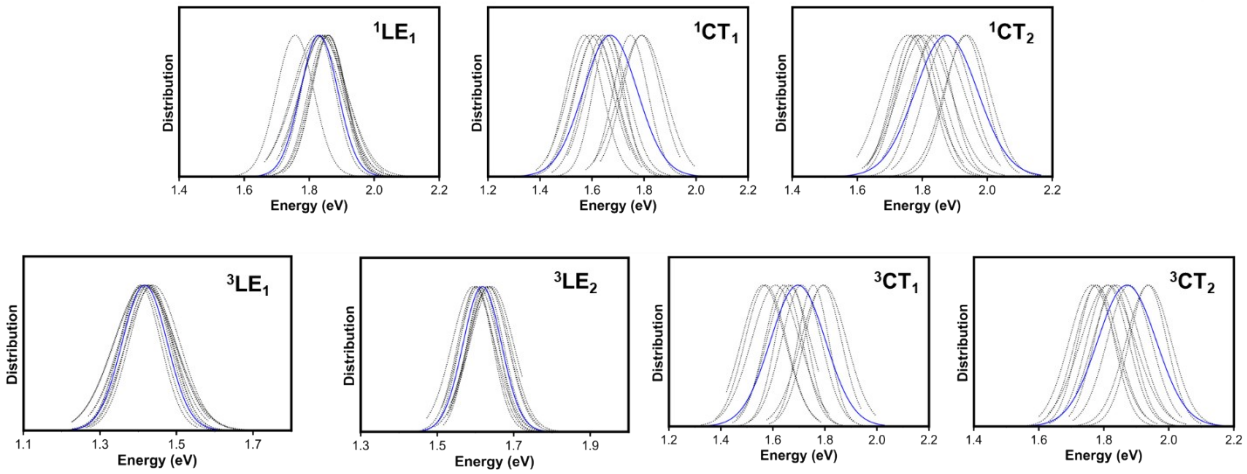

Figure S9: *Normalized distributions of total disorder including both static and dynamic contributions (blue lines) and of just dynamic disorder (black lines) for singlet and triplet LE and CT states. This analysis is based on 2000 PM6:Y6 complexes collected at 30 fs intervals from MD simulation trajectories.*

10. Origin of the defect states in PM6:Y6

As mentioned in the main text, it has been observed that ~0.4% PM6:Y6 pairs exhibit q $\leq$ 0.1 values in their S_1 state; additionally, their S_1 energies are found to be lower (typically below 1.60 eV), compared to the S_1 states of Y6 molecules or the LE states of the majority of PM6:Y6 complexes. Upon an in-depth analysis utilizing NTOs, we found that the S_1 states in these pairs, while having negligible PM6 to Y6 charge transfer, in fact exhibit *intra*-Y6 charge transfer (iY6-CT). This means that, while both the hole and electron are located within the Y6 molecule, the hole is typically located on the core moiety and the electron positioned on one of the terminal parts.

The considerable twist in the dihedral angle Φ within Y6 in these pairs plays a pivotal role in driving the occurrence of iY6-CT character in the S_1 states of these PM6:Y6 pairs.

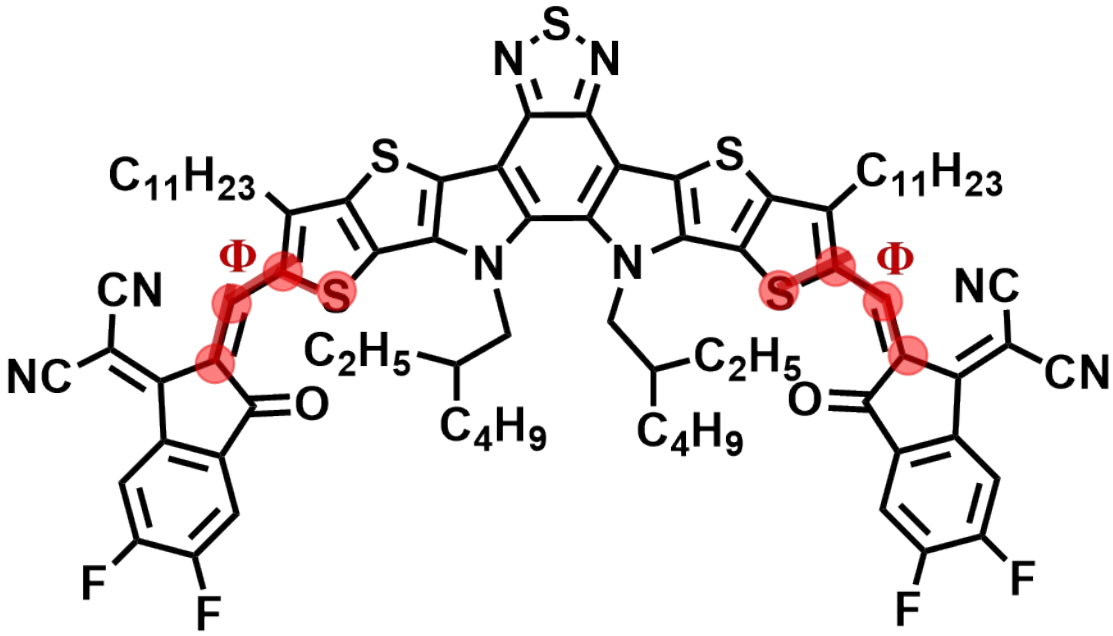

Figure S10: S*tructure of Y6 illustrating the dihedral angle (Φ) of interest.*

To further corroborate this observation, a single Y6 molecule was considered and its dihedral angle Φ (see Figure S10) was systematically rotated from its equilibrium geometry. As shown in Figure S11, the S_1 energy decreases as Φ is twisted, reaching a minimum around a perpendicular conformation of ~90° between the central and terminal Y6 segments. This suggests that the reduction in the S_1 energy of Y6 is indeed a consequence of the twisting of Φ. In addition to this, the Figure S12 illustrates how the wavefunctions of the hole and electron evolve in response to changes in Φ in this isolated Y6 molecule. It becomes evident that as Φ increases towards 90°, the prevalence of iY6-CT becomes more pronounced. For instance, at Φ= ~60°, a significant iY6-

CT feature emerges within Y6. However, at Φ= ~90°, the system exhibits complete iY6-CT, with this character gradually diminishing as Φ reaches above ~140°. This compelling evidence strongly suggests that the twisted Φ within Y6 is a key responsible for the iY6-CT characteristics.

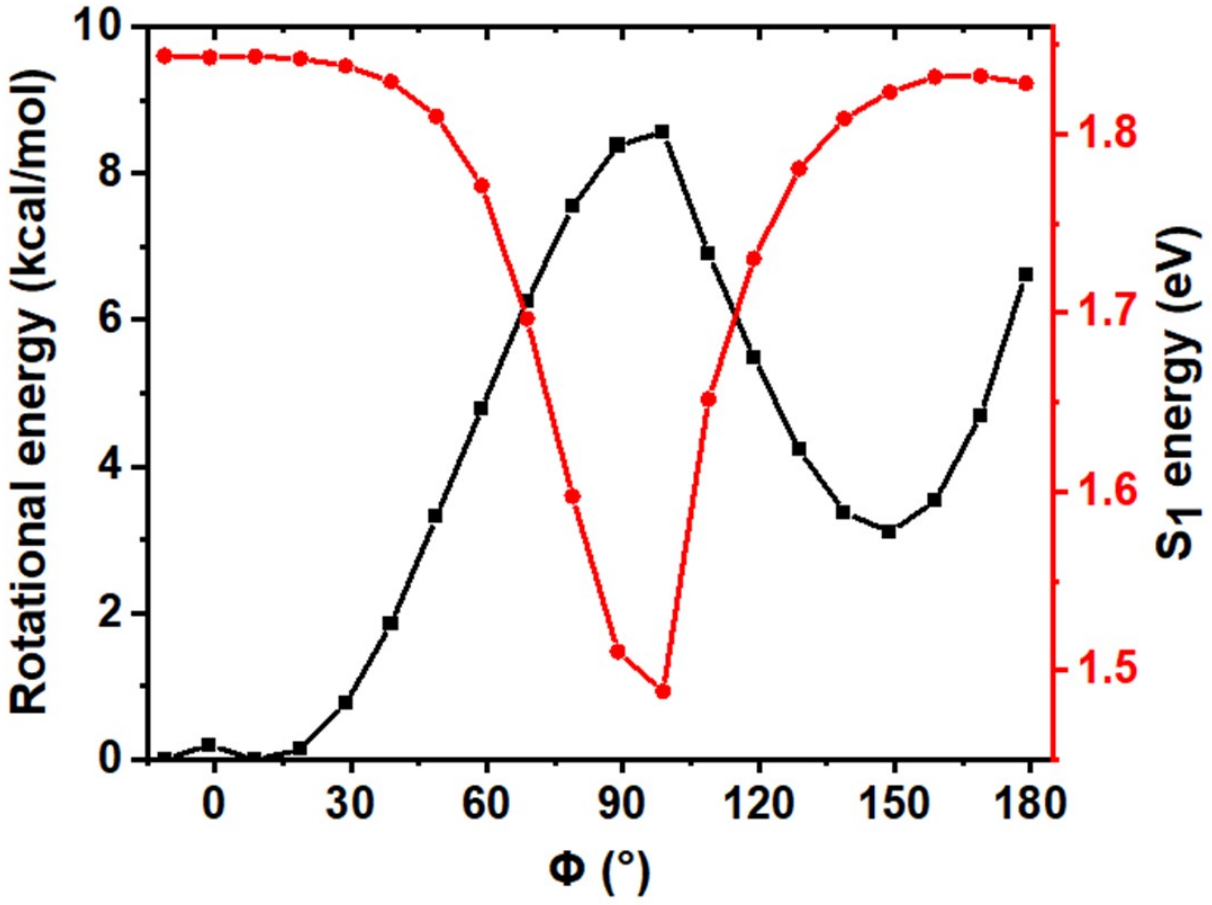

Figure S11: *Black line: Torsional energy related to dihedral angle Φ (in °) in Y6. Red line: Evolution of S_1 energy as a function of Φ. The rotational energies were calculated at the ωB97X-D/6-31G(d,p) level with ω=0.010 Bohr^{-1}, using the PCM model with ε=3.00 (Gaussian 16 package). The S_1 energies were calculated at the same level of theory (QChem 5.4 package).*

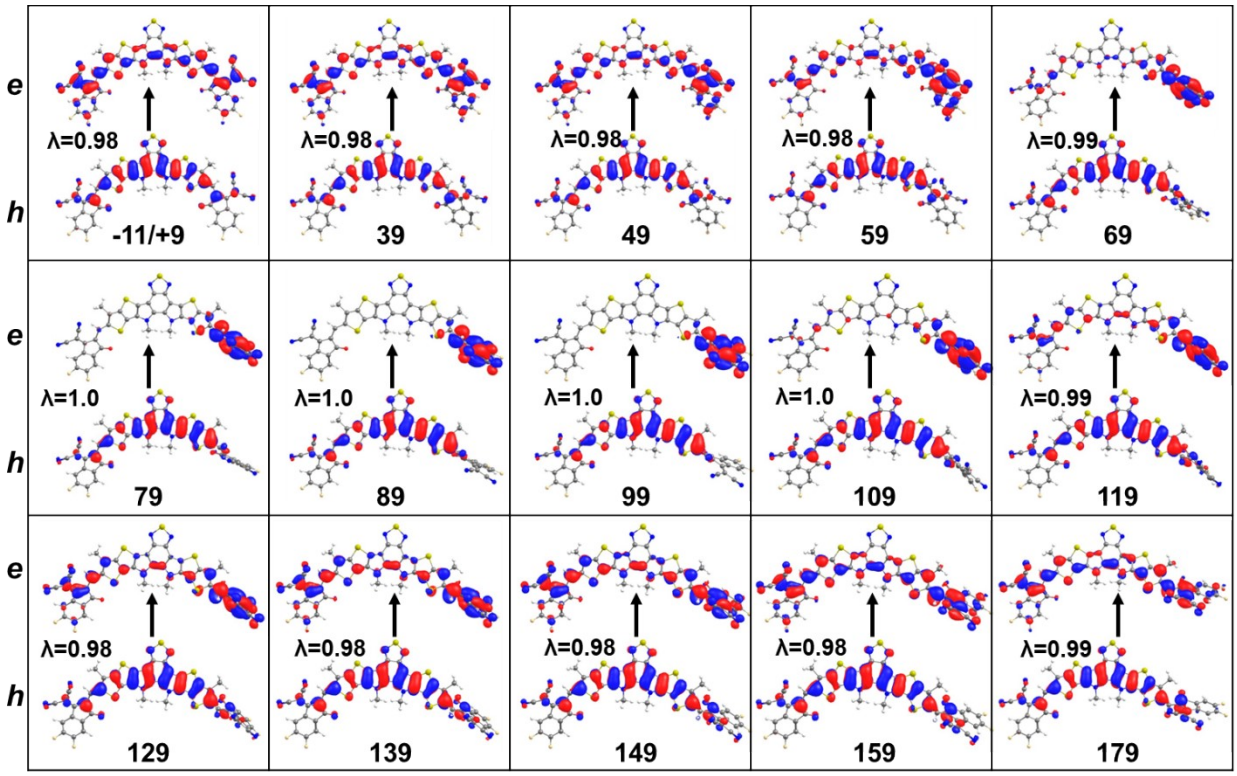

Figure S12: *Hole and electron NTOs for the Y6 S_1 state as a function of Φ (°). These calculations are carried out at the ωB97X-D/6-31G(d,p) level with ω=0.010 Bohr^{-1}, using the PCM model with ε=3.00 (Gaussian 16 package). The λ value indicates the weight of the NTO.*

Analysis of dihedral distribution of Y6 in PM6:Y6 blend

To gain insight into the variations in dihedral angle Φ (see Figure S10) in Y6, we collected the Φ angle values from all three distinct simulation boxes and constructed the corresponding histogram, depicted in Figure S13. This analysis reveals that the predominant distribution of Φ for Y6 molecules within the simulation boxes falls within the range of 0 to ±50°. However, it is interesting to note the existence of Y6 conformations that exhibit significant deviations in dihedral angles from the aforementioned range. These deviations can vary from ~ ±50° to ±180°, with a peak occurring around ±150°. Therefore, in view of the evolution of the CT character in single Y6 molecules (see Figure S11) and by examining the Φ distribution, it can be concluded that the lower-

energy S_1 states with $q \leq 0.1$ observed in PM6:Y6 result from Y6 conformations featuring Φ values in the range of ±60° to ±140° and are characterized by distinct iY6-CT features.

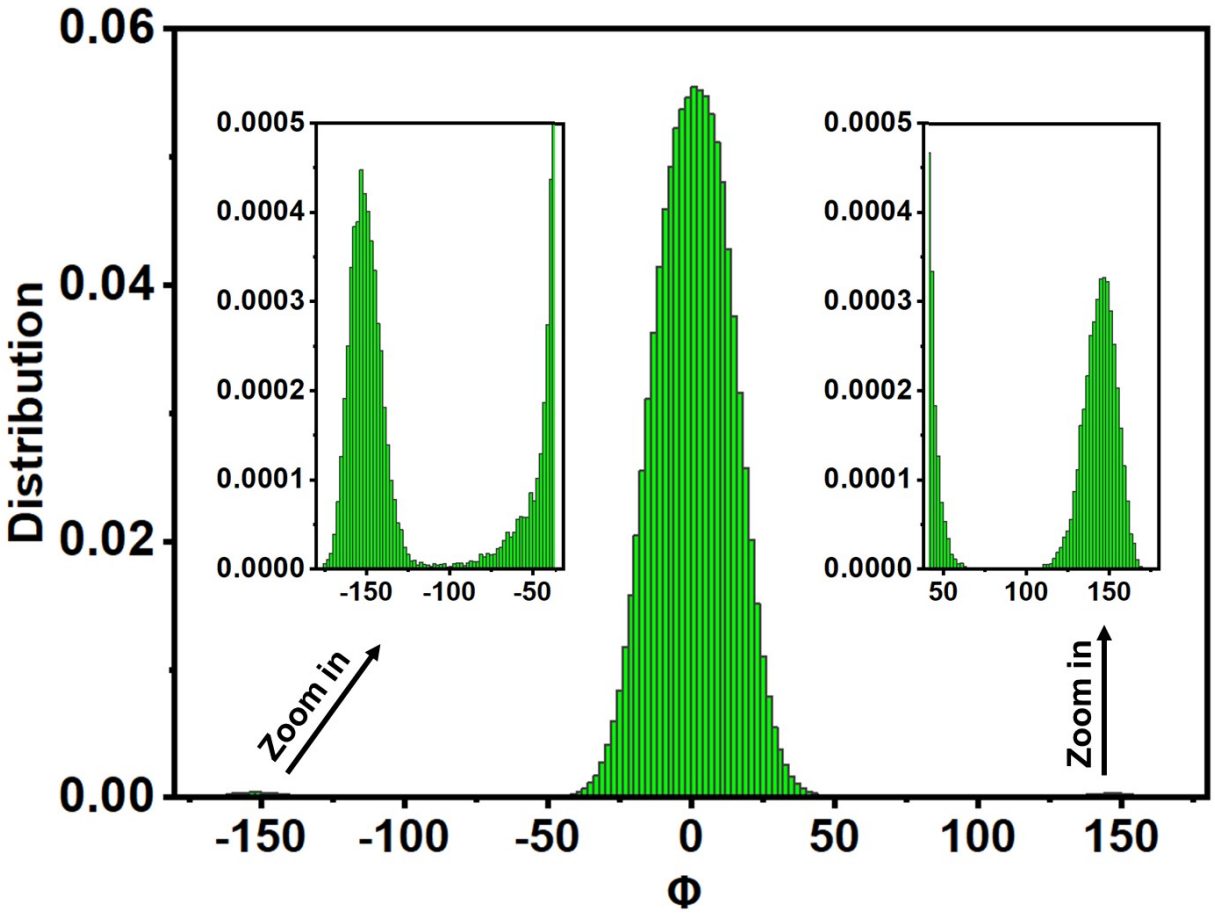

Figure S13: *Distribution of Φ values (in °) for the Y6 molecules in the PM6:Y6 blend as obtained from the MD simulations.*

Also, it is worth noting that the energy required to twist Φ in an isolated Y6 monomer is not very large (see Figure S11); for instance, ~4.8 kcal/mol energy is required for Φ to reach ~60°; to twist to a perpendicular conformation, *i.e.*, around Φ=90°, the energy requirement increases to ~8.6 kcal/mol (it should be kept in mind, however, that the rotation energy of an isolated Y6 monomer, as indicated in Figure S11, may differ from that of Y6 molecules within the blend due

to the influence of the surrounding molecules). In any event, it is possible that large dihedral angles appear during thermal annealing processes and may give rise to an iY6-CT character and low energy of the S_1 state. These low-energy states can then be a source of energy loss and lead to a reduction in PCE.

Section SD: Distributions of state energies and charges in 2Y6 and PM6:2Y6

11. Singlet and triplet energy distributions in Y6 dimer:

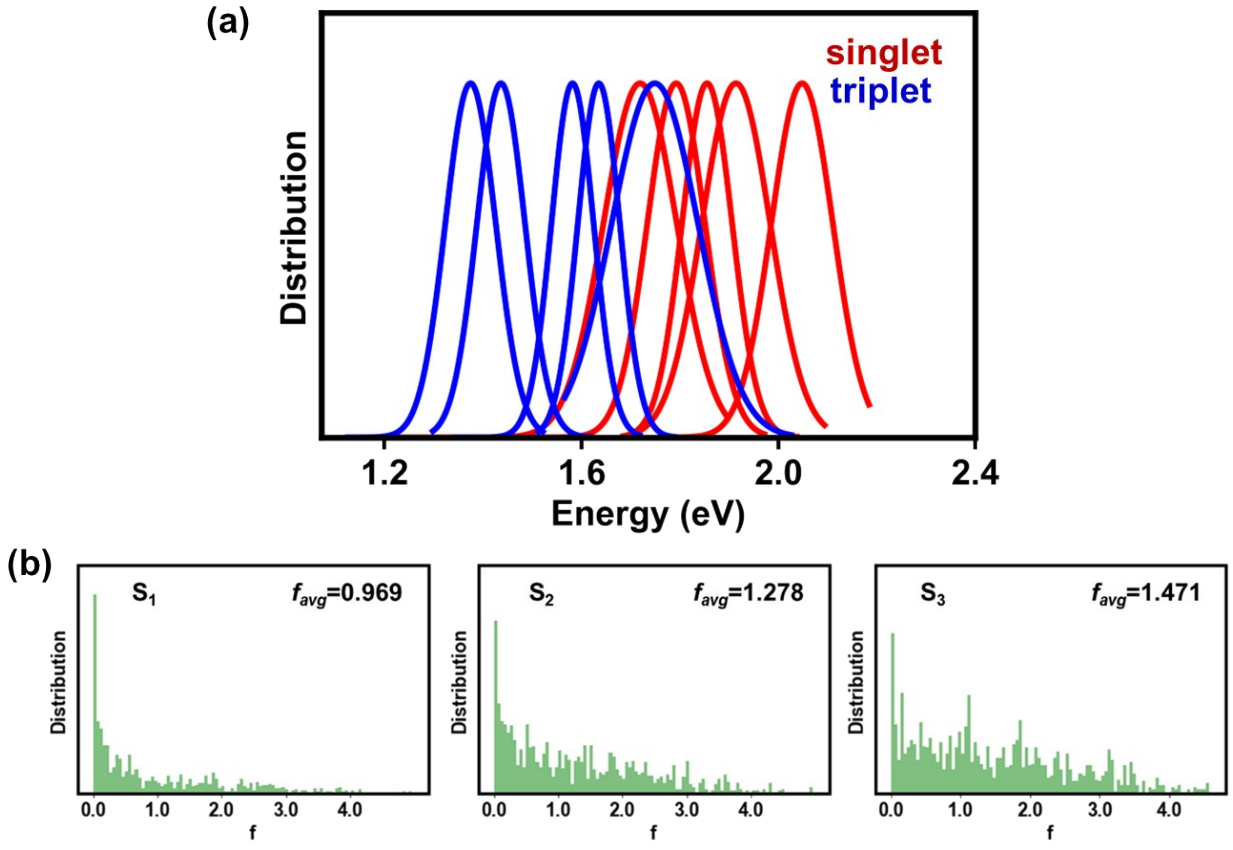

Figure S14: *(a) Normalized energy distribution of the five lowest-lying singlet and triplet states in a Y6 dimer based on 1000 pairs extracted from the MD simulations. Those Y6 dimers were*

obtained from the PM6:2Y6 complexes by excluding the PM6 component. Subsequently, TD-DFT calculations were conducted using the level of theory mentioned earlier. Triplet states are represented by blue lines and singlet states, by red lines. The average energy values of each state and their corresponding standard deviations are provided in Table S1. (b) Distribution of the oscillator strengths (f) for the S_1, S_2, and S_3 states of Y6 dimers, with f_{avg} indicating the average value.

12. Singlet and triplet energy distributions in PM6:2Y6:

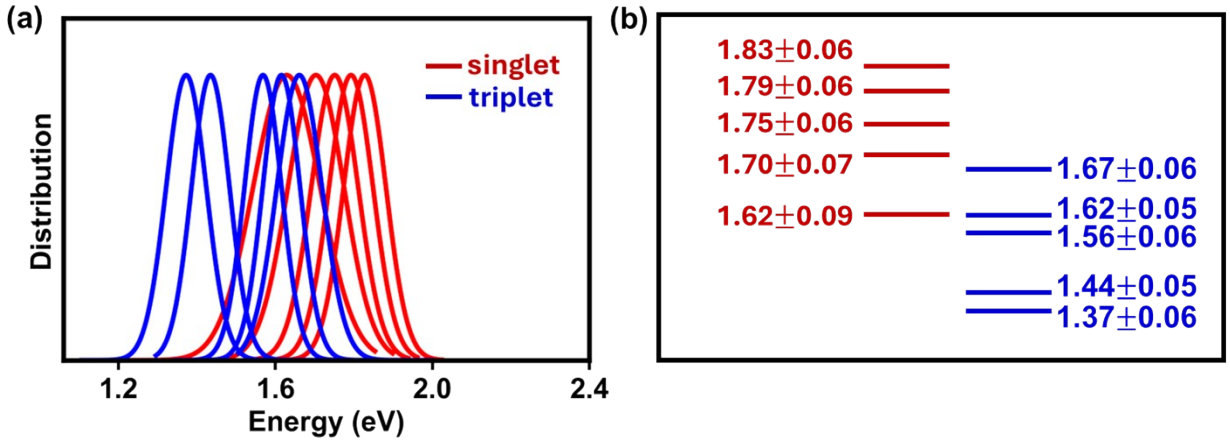

Figure S15: *(a) Normalized energy distributions for the five lowest-lying singlet and triplet states in PM6:2Y6 complexes based on 1500 MD extracted pairs. Subsequently, TD-DFT calculations were conducted using the level of theory mentioned earlier. Triplet states are represented by blue lines and singlet states, by red lines. (b) Average energy values of each singlet (red) and triplet (blue) state and their corresponding standard deviations.*

13. Distributions of charges in PM6:2Y6

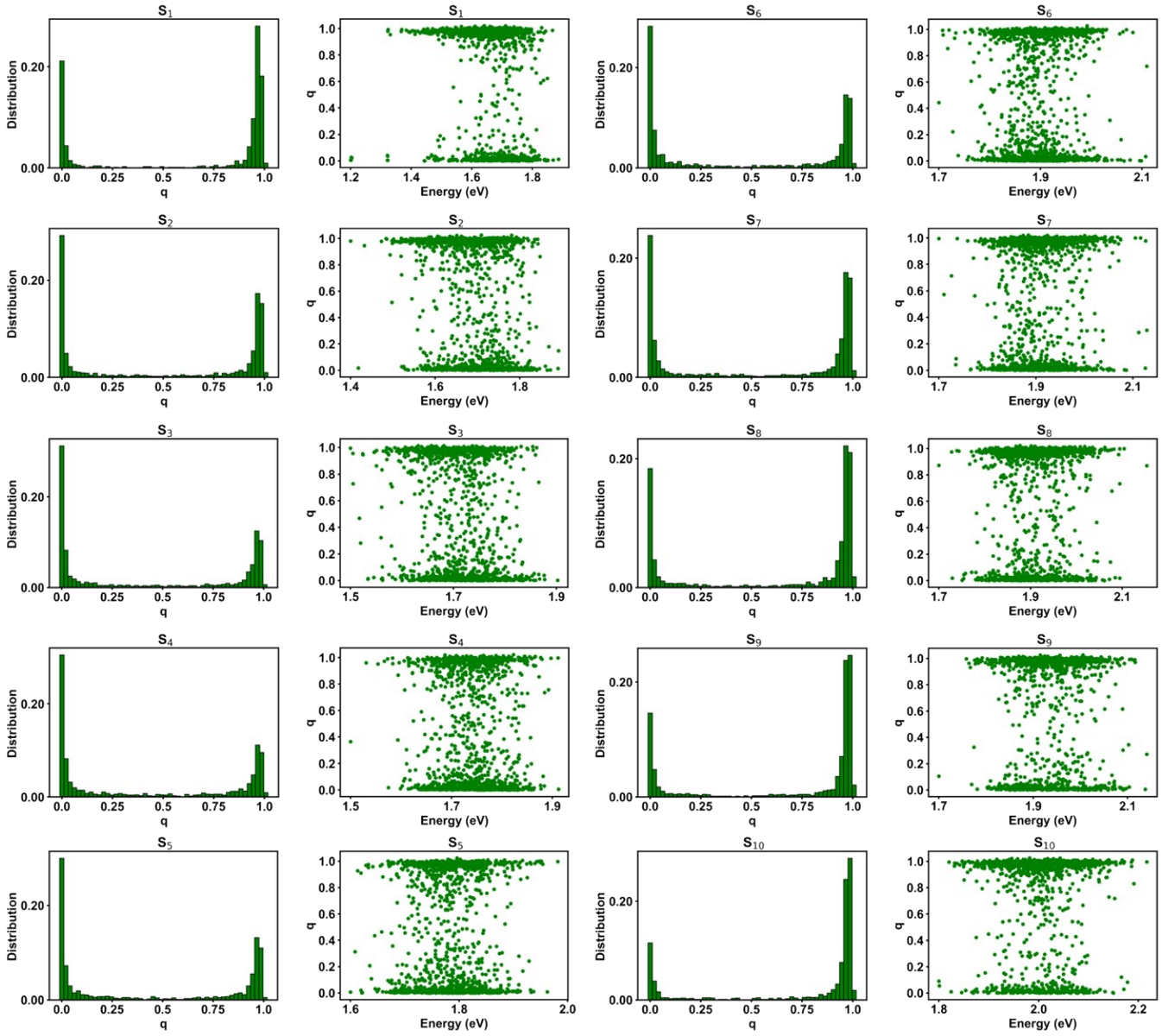

Figure S16: *Histogram plots of charges "q" and their distributions as a function of energy for various singlet states in the case of PM6:2Y6 complexes.*

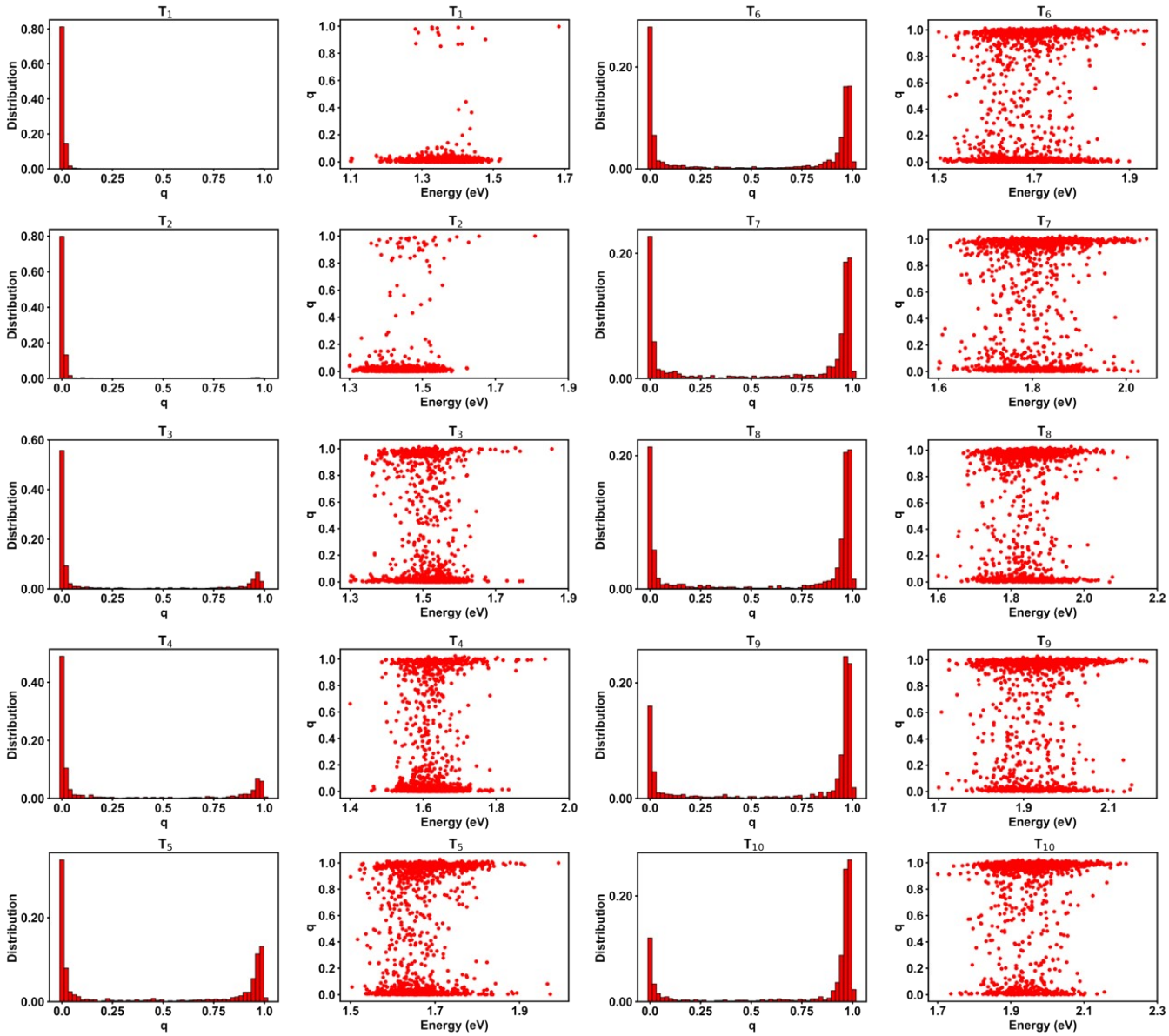

Figure S17: *Histogram plots of charges "q" and their distributions as a function of energy for various triplet states in the case of PM6:2Y6 complexes.*

14. Distributions of charges between two Y6 molecules within dimeric Y6 complexes

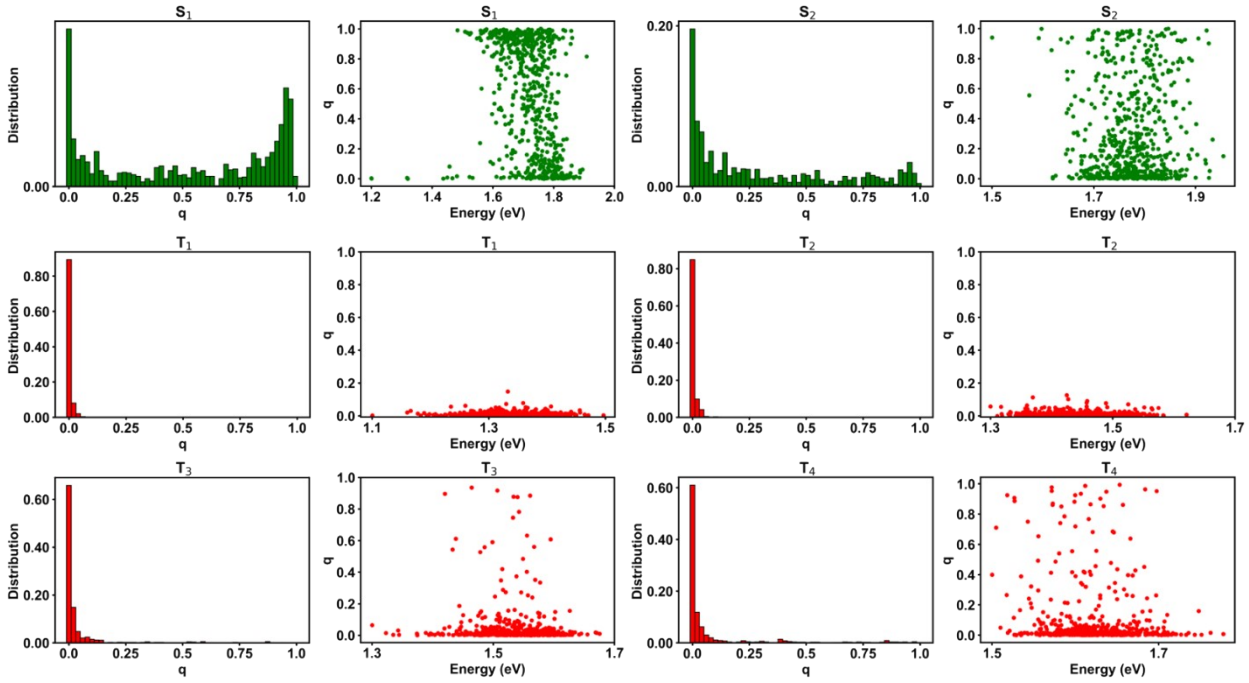

Figure S18: *Histogram plots of charges "q" and their distributions as a function of energy for various singlet and triplet states in the case of 2Y6 pairs. 1000 2Y6 pairs were extracted from PM6:2Y6 complexes by excluding PM6. The plots clearly illustrate that a considerable proportion of the S_1 states, which subsequently form the ^{1}EX state in PM6:2Y6 complexes, exhibit significant CT characteristics (q≥0.9), indicative of inter-Y6 CT; however, a substantial number of 2Y6 pairs possess a local excitonic character (q≤0.1). Similarly, the S_2 state manifests a mixture of local and CT characteristics. In contrast, the lowest four triplet states, which subsequently form the four lowest-lying triplet LE states in PM6:2Y6 complexes, completely lack CT characteristics and solely possess LE behavior.*

15. Energy offsets between singlet CT and triplet CT states in Y6 pairs

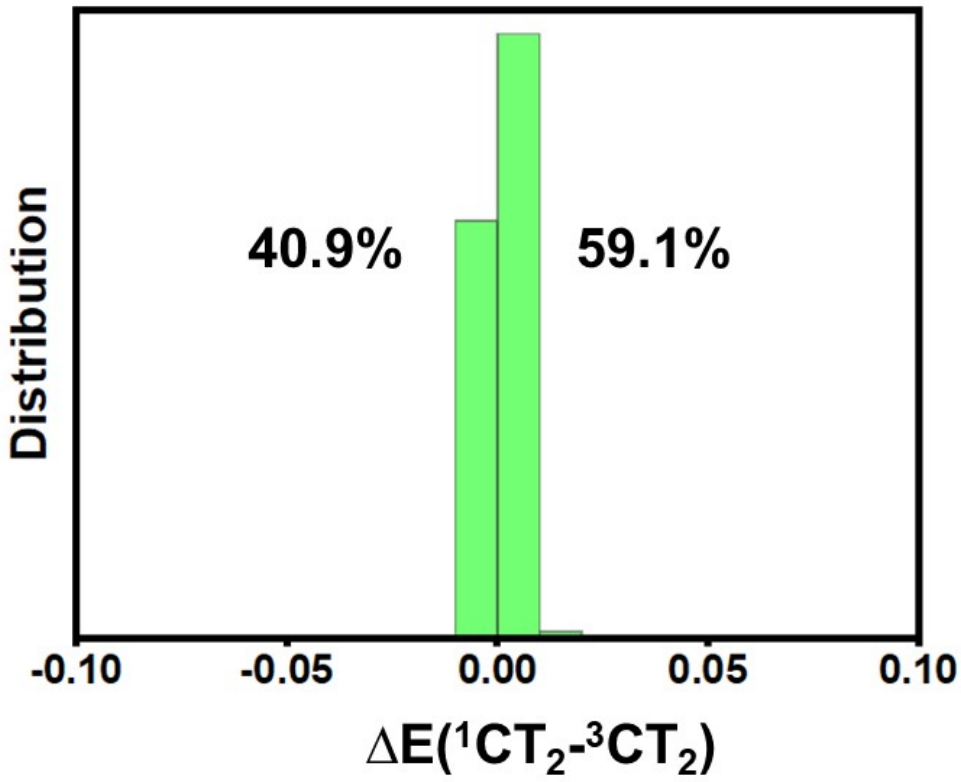

Figure S19: *Distribution of energy offsets (in eV) between singlet and triplet CT states [$\Delta E(^1CT_2$-$^3CT_2)$] across individual complexes for PM6:2Y6. The percentage of complexes showing positive and negative energy offsets are also provided.*

16. Singlet and triplet LE and CT states

Table S3: *Average energies and standard deviations for the singlet and triplet LE/EX and CT states in PM6:Y6 and PM6:2Y6 complexes.*

	PM6:Y6		PM6:2Y6	
States	E_{avg}	σ	E_{avg}	σ
$^1LE_1$ ($^1EX_1$)	1.84	0.08	1.72	0.10
$^1LE_2$ ($^1EX_2$)			1.80	0.07
$^1LE_3$ ($^1EX_3$)	--	--	1.87	0.07
$^1LE_4$ ($^1EX_4$)	--	--	1.92	0.08
$^1CT_1$	1.67	0.11	1.63	0.11
$^1CT_2$	1.87	0.10	1.74	0.10
$^1CT_3$	1.97	0.09	1.84	0.09
$^3LE_1$ ($^3EX_1$)	1.42	0.07	1.41	0.07
$^3LE_2$ ($^3EX_2$)	1.62	0.07	1.63	0.09
$^3LE_3$ ($^3EX_3$)	1.83	0.10	1.77	0.09
$^3CT_1$	1.69	0.11	1.66	0.11
$^3CT_2$	1.87	0.09	1.76	0.10
$^3CT_3$	1.95	0.10	1.83	0.10

Section SE: Origin of LE States in PM6:Y6 and PM6:2Y6

17. Lowest singlet and triplet states in Y6[2Y6] vs. LE states in PM6:Y6 [PM6:2Y6]

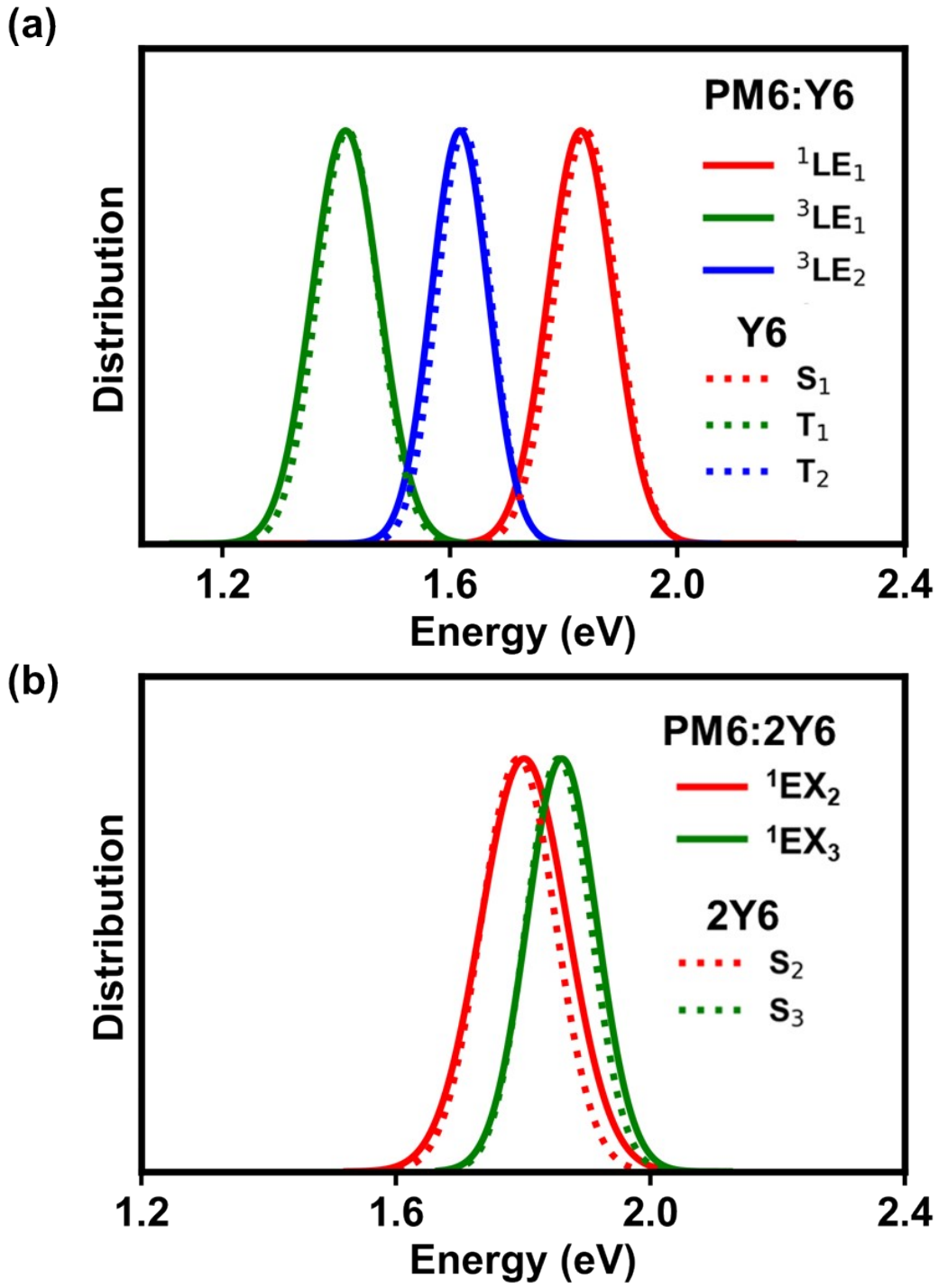

Figure S20: *(a) Normalized energy distributions for singlet and triplet LE states in PM6:Y6 complexes, superimposed on the energy distributions for Y6 molecules. (b) Normalized energy distributions for singlet EX states in PM6:2Y6 complexes superimposed on the energy distributions for 2Y6 dimers. Also see Figure 4 in the main text for the triplet EX states in PM6:2Y6 complexes vs 2Y6 dimers. In PM6:Y6 complexes, the $^1LE_1$, $^3LE_1$, and $^3LE_2$ states overlap completely with the energy distributions of the S_1, T_1, and T_2 states of Y6 molecules, respectively. Likewise, in PM6:2Y6 complexes, the $^1EX_1$, $^1EX_2$, and $^1EX_3$ states coincide entirely with the energy distributions of the S_1, S_2, and S_3 states, and the $^3EX_1$ and $^3EX_2$ states coincide with the T_1 and T_2 states of 2Y6, respectively. These observations indicate that the lower-energy singlet and triplet states of the Y6 molecules and 2Y6 pairs remain unchanged during blend formation. They exclusively contribute to the formation of LE states in the blend.*

Section SF: Distributions of oscillator strengths and couplings

18. Distributions of oscillator strengths for PM6:Y6 and PM6:2Y6

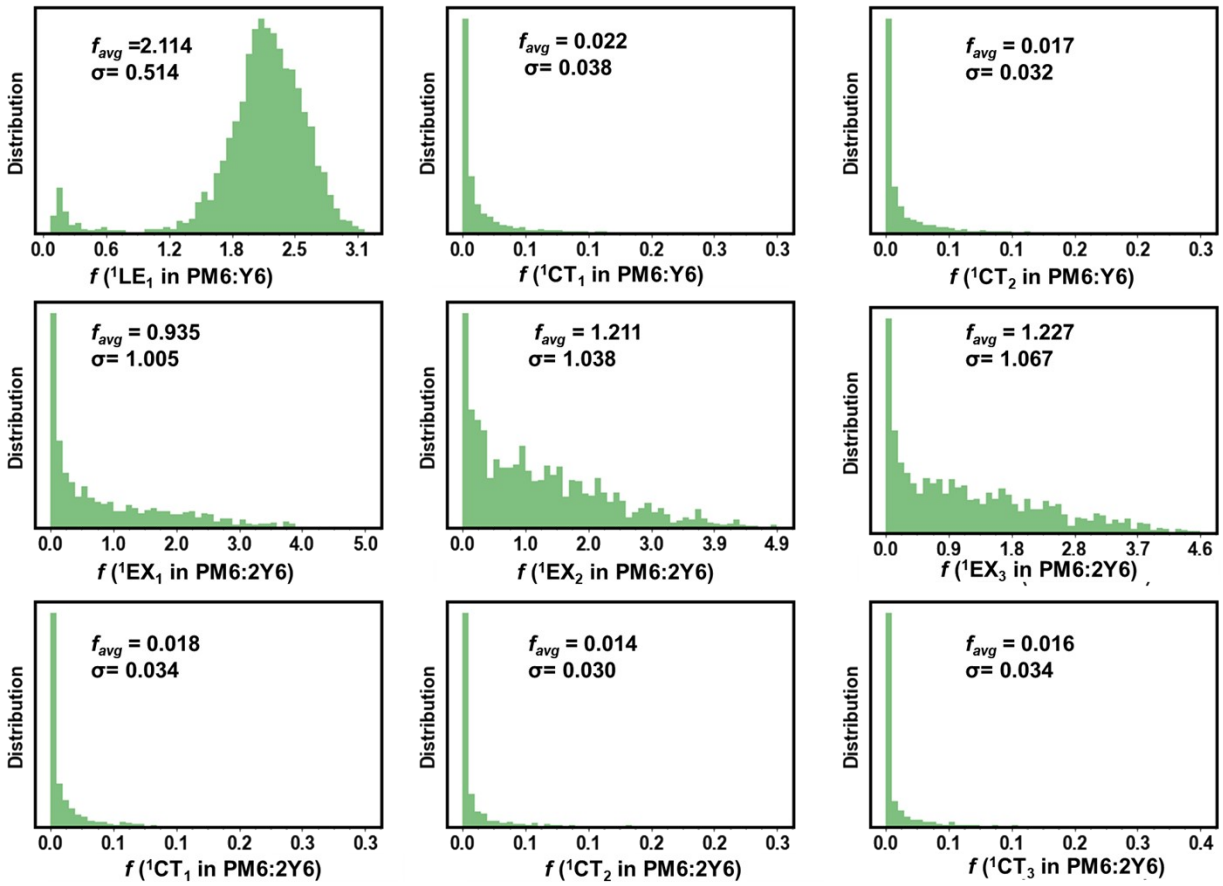

Figure S21: *Distributions of oscillator strength (f) of ^{1}LE/^{1}EX and ^{1}CT state in PM6:Y6 and PM6:2Y6, with the average value [f_{avg}] and standard deviation (σ).*

19. Distributions of spin-orbit couplings

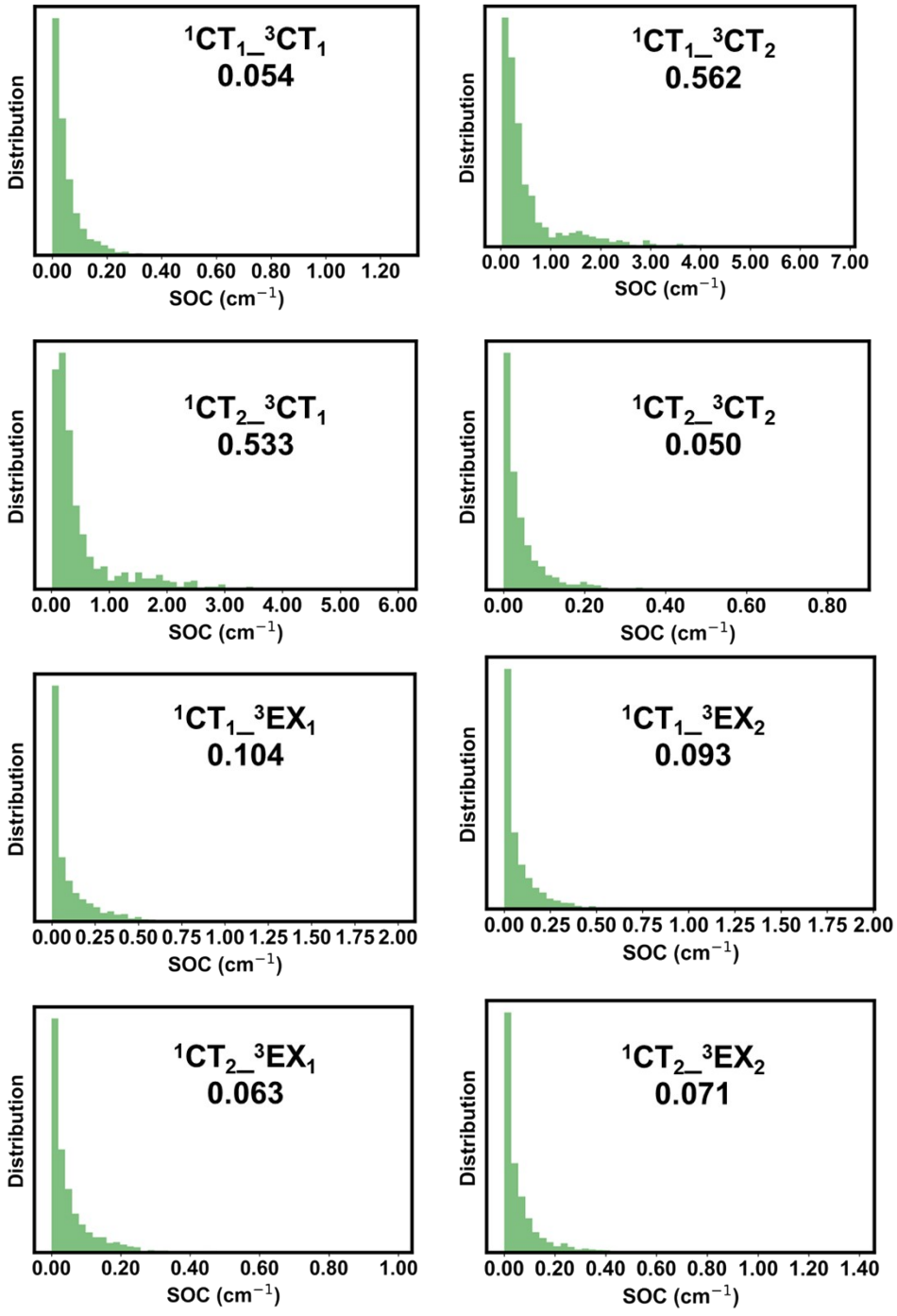

Figure S22: *Distributions of spin-orbit couplings (SOC) among ^{1}CT and ^{3}CT states and among ^{1}CT and ^{3}EX states for PM6:2Y6 complexes. The corresponding average values are shown in each plot.*

20. Distributions of electronic couplings

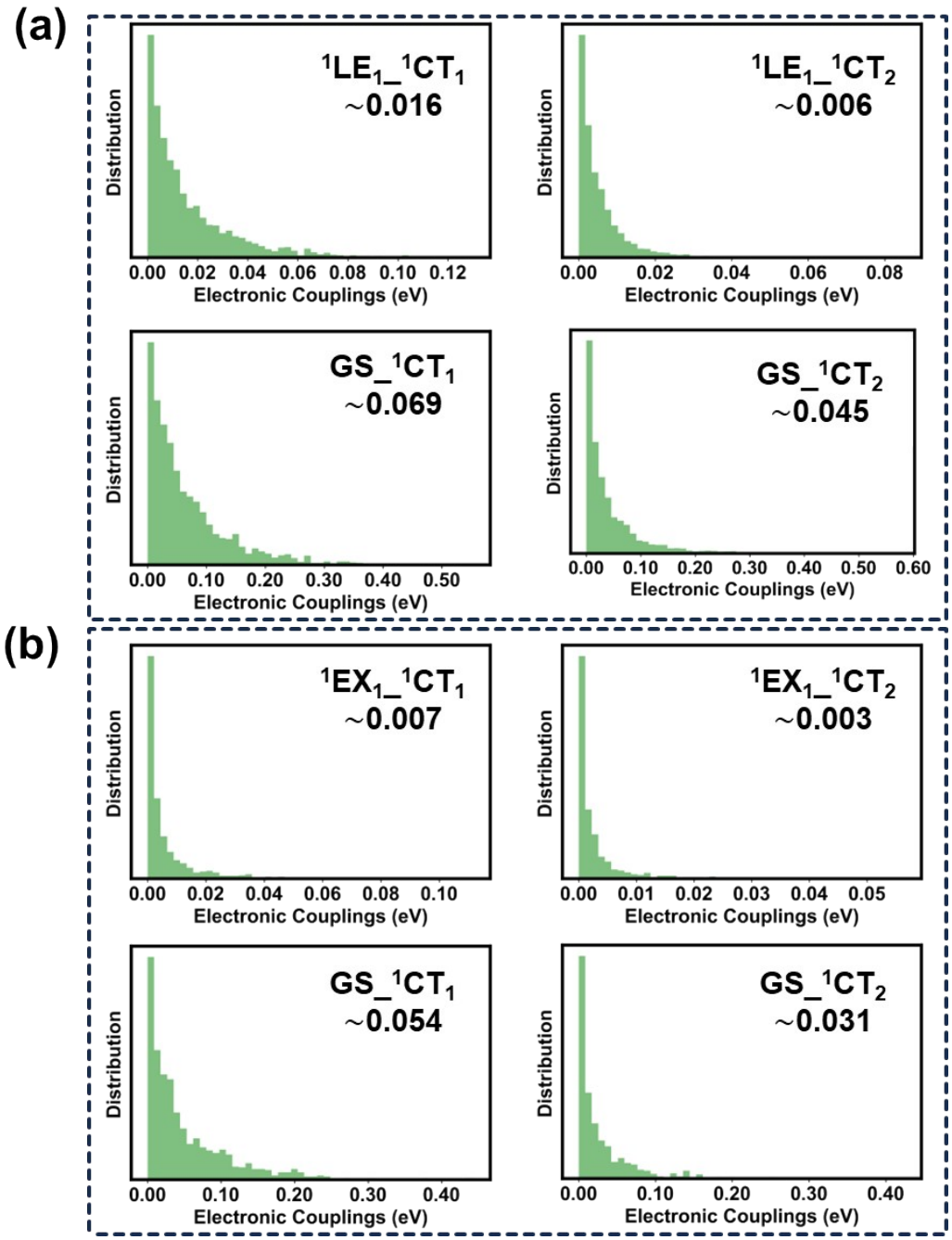

Figure S23: *Distributions of the electronic couplings between the ^{1}LE(^{1}EX) and ^{1}CT states, and between the ground state and ^{1}CT states for the (a) PM6:Y6 and (b) PM6:2Y6 complexes.*

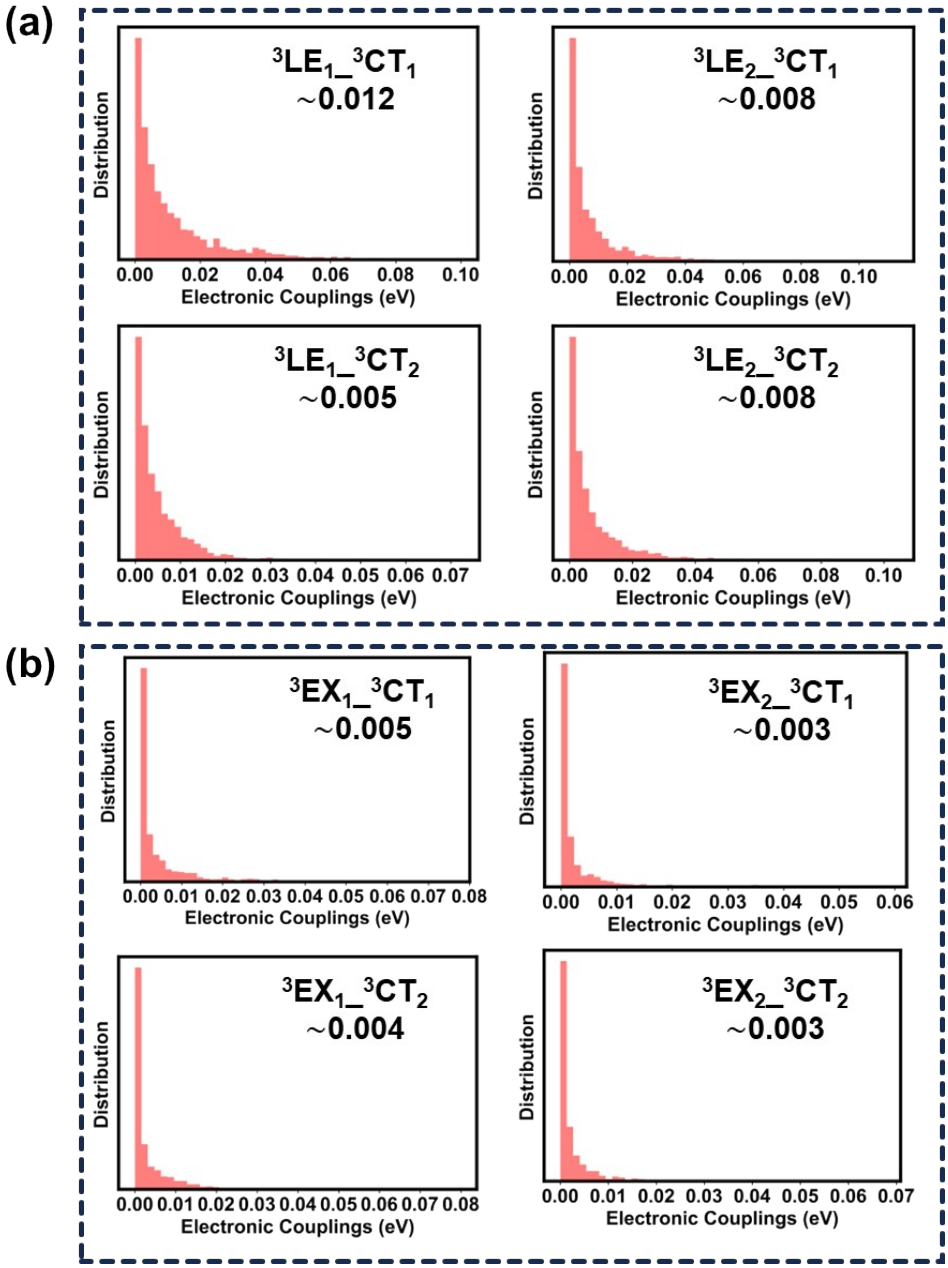

Figure S24: *Distributions of electronic couplings between ^{3}LE(^{3}EX) and ^{3}CT states in PM6:Y6 and PM6:2Y6 complexes. Their average values are also reported.*

Section SG: Fate of LE triplet state

21. Rates of local triplet state formation from triplet CT state and reverse rates

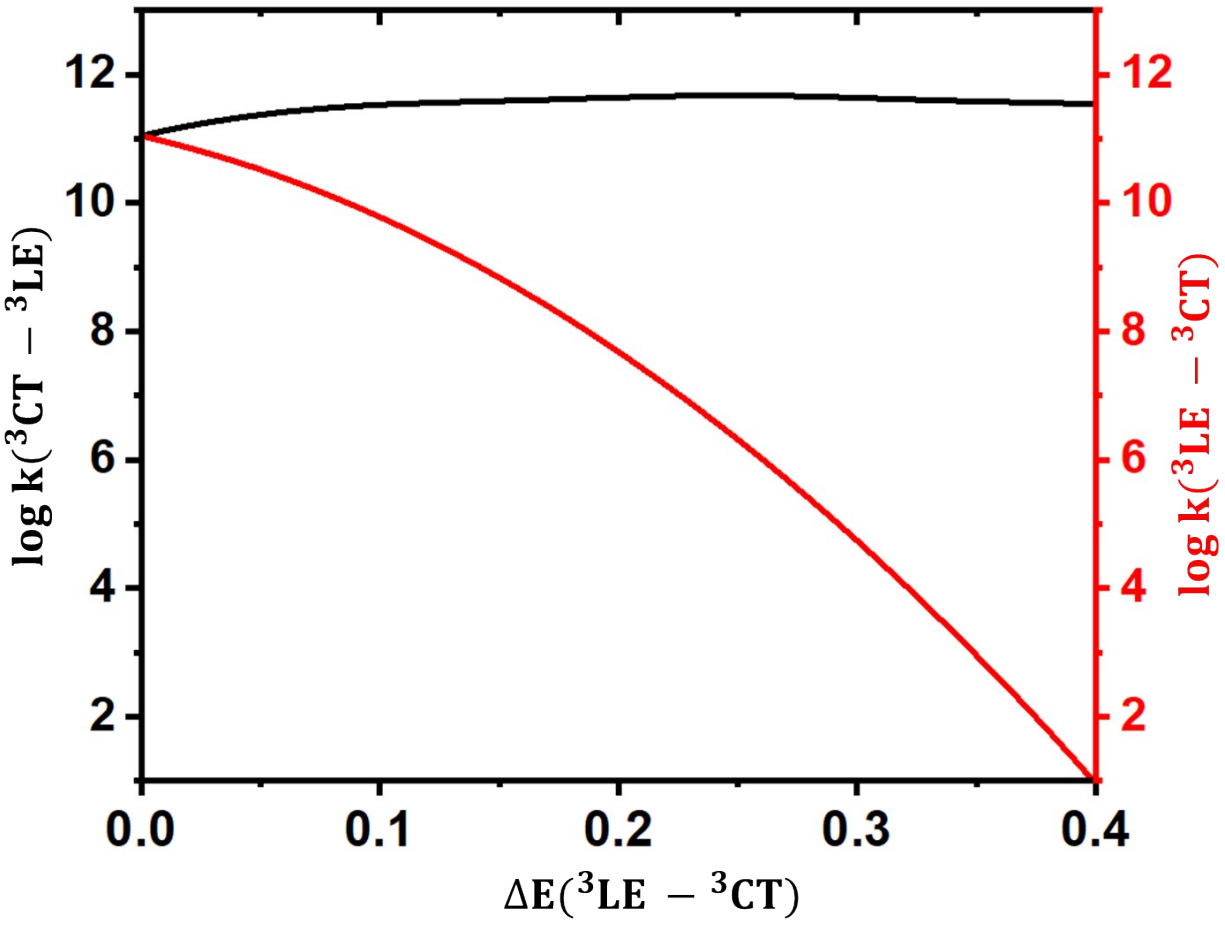

Figure S25: *Rate of formation of the ^{3}LE state from the ^{3}CT state (in black) and reverse rate from the ^{3}LE state to the ^{3}CT state (in red), as a function of the ^{3}LE-^{3}CT energy splitting.*

Section SH: Rate calculations

22. Parameters for rate calculations

Table S4: *Calculated values of classical reorganization energy (λ_c), reorganization energy associated with high frequency modes (λ_{qm}), and Huang-Rhys factor (S_{qm}), as obtained at the ωb97XD/6-31G(d,p) level (ω=0.01 Bohr-1, PCM model with ε=3).*

Parameters	^{1}LE-^{1}CT	^{1}CT-GS	^{3}CT-^{3}LE	^{3}LE-GS	^{1}CT-CS
λ_c (eV)	0.1	0.1	0.1	0.1	0.12
λ_{qm} (eV)	0.15	0.15	0.15	0.16	0.15
S_{qm}	1.40	1.40	1.40	0.72	1.96

Section SI: References:

1. S. Plimpton, *Journal of Computational Physics*, 1995, **117**, 1-19.
2. W. L. Jorgensen and J. Tirado-Rives, *Journal of the American Chemical Society*, 1988, **110**, 1657-1666.
3. M. K. Dahlgren, P. Schyman, J. Tirado-Rives and W. L. Jorgensen, *Journal of Chemical Information and Modeling*, 2013, **53**, 1191-1199.
4. N. E. Jackson, K. L. Kohlstedt, B. M. Savoie, M. Olvera de la Cruz, G. C. Schatz, L. X. Chen and M. A. Ratner, *Journal of the American Chemical Society*, 2015, **137**, 6254-6262.
5. J.-D. Chai and M. Head-Gordon, *Physical Chemistry Chemical Physics*, 2008, **10**, 6615-6620.
6. F. Weigend and R. Ahlrichs, *Physical Chemistry Chemical Physics*, 2005, **7**, 3297-3305.
7. W. J. Hehre, R. Ditchfield and J. A. Pople, *The Journal of Chemical Physics*, 1972, **56**, 2257-2261.
8. M. J. Frisch, G. W. Trucks, H. B. Schlegel, G. E. Scuseria, M. A. Robb, J. R. Cheeseman, G. Scalmani, V. Barone, G. A. Petersson, H. Nakatsuji, X. Li, M. Caricato, A. V. Marenich, J. Bloino, B. G. Janesko, R. Gomperts, B. Mennucci, H. P. Hratchian, J. V. Ortiz, A. F. Izmaylov, J. L. Sonnenberg, Williams, F. Ding, F. Lipparini, F. Egidi, J. Goings, B. Peng, A. Petrone, T. Henderson, D. Ranasinghe, V. G. Zakrzewski, J. Gao, N. Rega, G. Zheng, W. Liang, M. Hada, M. Ehara, K. Toyota, R. Fukuda, J. Hasegawa, M. Ishida, T. Nakajima, Y. Honda, O. Kitao, H. Nakai, T. Vreven, K. Throssell, J. A. Montgomery Jr., J. E. Peralta, F. Ogliaro, M. J. Bearpark, J. J. Heyd, E. N. Brothers, K. N. Kudin, V. N. Staroverov, T. A. Keith, R. Kobayashi, J. Normand, K. Raghavachari, A. P. Rendell, J. C. Burant, S. S. Iyengar, J. Tomasi, M. Cossi, J. M. Millam, M. Klene, C. Adamo, R. Cammi, J. W. Ochterski, R. L. Martin, K. Morokuma, O. Farkas, J. B. Foresman and D. J. Fox, *Journal*, 2016.
9. L. J. Abbott, K. E. Hart and C. M. Colina, *Theoretical Chemistry Accounts*, 2013, **132**, 1334.
10. M. E. Fortunato and C. M. Colina, *SoftwareX*, 2017, **6**, 7-12.
11. G. Kupgan, X. K. Chen and J. L. Brédas, *Materials Today Advances*, 2021, **11**, 100154.
12. N. R. Tummala, S. A. Elroby, S. G. Aziz, C. Risko, V. Coropceanu and J.-L. Brédas, *The Journal of Physical Chemistry C*, 2016, **120**, 17242-17250.
13. N. R. Tummala, Z. Zheng, S. G. Aziz, V. Coropceanu and J.-L. Brédas, *The Journal of Physical Chemistry Letters*, 2015, **6**, 3657-3662.
14. Z. Zheng, N. R. Tummala, T. Wang, V. Coropceanu and J.-L. Brédas, *Advanced Energy Materials*, 2019, **9**, 1803926.
15. C. He, Z. Chen, T. Wang, Z. Shen, Y. Li, J. Zhou, J. Yu, H. Fang, Y. Li, S. Li, X. Lu, W. Ma, F. Gao, Z. Xie, V. Coropceanu, H. Zhu, J.-L. Bredas, L. Zuo and H. Chen, *Nature Communications*, 2022, **13**, 2598.
16. T. Wang, V. Coropceanu and J.-L. Brédas, *Chemistry of Materials*, 2019, **31**, 6239-6248.
17. D. Qian, S. M. Pratik, Q. Liu, Y. Dong, R. Zhang, J. Yu, N. Gasparini, J. Wu, T. Zhang, V. Coropceanu, X. Guo, M. Zhang, J.-L. Bredas, F. Gao and J. R. Durrant, *Advanced Energy Materials*, 2023, **13**, 2301026.
18. A. A. Voityuk and N. Rösch, *The Journal of Chemical Physics*, 2002, **117**, 5607-5616.
19. R. J. Cave and M. D. Newton, *Chemical Physics Letters*, 1996, **249**, 15-19.

20. Y. Shao, Z. Gan, E. Epifanovsky, A. T. B. Gilbert, M. Wormit, J. Kussmann, A. W. Lange, A. Behn, J. Deng, X. Feng, D. Ghosh, M. Goldey, P. R. Horn, L. D. Jacobson, I. Kaliman, R. Z. Khaliullin, T. Kuś, A. Landau, J. Liu, E. I. Proynov, Y. M. Rhee, R. M. Richard, M. A. Rohrdanz, R. P. Steele, E. J. Sundstrom, H. L. Woodcock, P. M. Zimmerman, D. Zuev, B. Albrecht, E. Alguire, B. Austin, G. J. O. Beran, Y. A. Bernard, E. Berquist, K. Brandhorst, K. B. Bravaya, S. T. Brown, D. Casanova, C.-M. Chang, Y. Chen, S. H. Chien, K. D. Closser, D. L. Crittenden, M. Diedenhofen, R. A. DiStasio, H. Do, A. D. Dutoi, R. G. Edgar, S. Fatehi, L. Fusti-Molnar, A. Ghysels, A. Golubeva-Zadorozhnaya, J. Gomes, M. W. D. Hanson-Heine, P. H. P. Harbach, A. W. Hauser, E. G. Hohenstein, Z. C. Holden, T.-C. Jagau, H. Ji, B. Kaduk, K. Khistyaev, J. Kim, J. Kim, R. A. King, P. Klunzinger, D. Kosenkov, T. Kowalczyk, C. M. Krauter, K. U. Lao, A. D. Laurent, K. V. Lawler, S. V. Levchenko, C. Y. Lin, F. Liu, E. Livshits, R. C. Lochan, A. Luenser, P. Manohar, S. F. Manzer, S.-P. Mao, N. Mardirossian, A. V. Marenich, S. A. Maurer, N. J. Mayhall, E. Neuscamman, C. M. Oana, R. Olivares-Amaya, D. P. O'Neill, J. A. Parkhill, T. M. Perrine, R. Peverati, A. Prociuk, D. R. Rehn, E. Rosta, N. J. Russ, S. M. Sharada, S. Sharma, D. W. Small, A. Sodt, T. Stein, D. Stück, Y.-C. Su, A. J. W. Thom, T. Tsuchimochi, V. Vanovschi, L. Vogt, O. Vydrov, T. Wang, M. A. Watson, J. Wenzel, A. White, C. F. Williams, J. Yang, S. Yeganeh, S. R. Yost, Z.-Q. You, I. Y. Zhang, X. Zhang, Y. Zhao, B. R. Brooks, G. K. L. Chan, D. M. Chipman, C. J. Cramer, W. A. Goddard, M. S. Gordon, W. J. Hehre, A. Klamt, H. F. Schaefer, M. W. Schmidt, C. D. Sherrill, D. G. Truhlar, A. Warshel, X. Xu, A. Aspuru-Guzik, R. Baer, A. T. Bell, N. A. Besley, J.-D. Chai, A. Dreuw, B. D. Dunietz, T. R. Furlani, S. R. Gwaltney, C.-P. Hsu, Y. Jung, J. Kong, D. S. Lambrecht, W. Liang, C. Ochsenfeld, V. A. Rassolov, L. V. Slipchenko, J. E. Subotnik, T. Van Voorhis, J. M. Herbert, A. I. Krylov, P. M. W. Gill and M. Head-Gordon, *Molecular Physics*, 2015, **113**, 184-215.
21. R. C. Hilborn, *American Journal of Physics*, 1982, **50**, 982-986.
22. J.-L. Brédas, D. Beljonne, V. Coropceanu and J. Cornil, *Chemical Reviews*, 2004, **104**, 4971-5004.
23. J. Jortner, *The Journal of Chemical Physics*, 2008, **64**, 4860-4867.